AN ANALYTICAL AND EXPERIMENTAL INVESTIGATION INTO THE APPLICATION OF A POLYPHASE TRANSISTOR SWITCHING CIRCUIT FOR SPEED CONTROL OF INDUCTION MOTORS

John M. Dorsey
and
Randolph D. Zelov

AN ANALYTICAL AND EXPERIMENTAL INVESTIGATION INTO THE APPLICATION OF A POLYPHASE TRANSISTOR SWITCHING CIRCUIT FOR SPEED CONTROL OF INDUCTION MOTORS

by

John Michael Dorsey, Lieutenant Commander,
U. S. Coast Guard
B.S., U. S. Coast Guard Academy, 1944

Randolph Dickinson Zelov, Lieutenant,
U. S. Navy
B.S., U. S. Naval Academy, 1947

and

Robert Lee Krag, Lieutenant, U. S. Navy
B.S., U. S. Naval Academy, 1950

SUBMITTED IN PARTIAL FULFILLMENT OF THE REQUIREMENTS FOR THE DEGREE OF NAVAL ENGINEER

at the

MASSACHUSETTS INSTITUTE OF TECHNOLOGY

June, 1956

Cambridge, Massachusetts

May 21, 1956

Professor Leicester F. Hamilton
Secretary of the Faculty
Massachusetts Institute of Technology
Cambridge, Massachusetts

Dear Professor Hamilton:

In accordance with the requirements for the Degree of Naval Engineer, we submit herewith a thesis entitled: "An Analytical and Experimental Investigation into the Application of a Polyphase Transistor Switching Circuit for Speed Control of Induction Motors."

Respectfully yours,

AN ANALYTICAL AND EXPERIMENTAL INVESTIGATION INTO THE APPLICATION OF A POLYPHASE TRANSISTOR SWITCHING CIRCUIT FOR SPEED CONTROL OF INDUCTION MOTORS

by

John Michael Dorsey
Lieutenant Commander, U. S. Coast Guard

Randolph Dickinson Zelov
Lieutenant, U. S. Navy

and

Robert Lee Krag
Lieutenant, U. S. Navy

Submitted to the Department of Naval Architecture and Marine Engineering on May 21, 1956 in partial fulfillment of the requirements for the degree of Naval Engineer

ABSTRACT

The polyphase switching-transistor circuit studied in this thesis offers promise of attaining speed control of induction motors by providing a simple means of varying line frequency. Both by theoretical analysis and in experimental work, the practicability of such an application is proved. While problems do exist, viz., undesirable rotor heating due to harmonic content in the switching-circuit output, possibility of difficulty in starting the motor due to the low impedance of an induction motor at starting, and relatively low power levels obtainable from presently available power transistors, all these difficulties are capable of solution.

The theoretical analysis includes a study of operation of the single-phase circuit based on operation as a relaxation oscillator. Then, the effect of adding more phases is studied. These analyses point out the importance of various circuit parameters in determining range of circuit operation.

The procedure for designing a three-phase circuit is outlined and the problems encountered in attempting to attain maximum power output are discussed.

The feasibility of utilizing the switching-circuit output as a power supply for a conventional induction motor is investigated analytically. The most important subjects studied are the effects of harmonic content in applied voltage on torque-speed characteristics of the motor and the additional rotor copper losses which result due to this harmonic content.

The experimental work consists of designing a three-phase circuit and making it operate. Experimental data obtained deals primarily with the effect of various circuit parameters on operation, providing confirmation of the predictions of theory. A synchro, with shorted rotor, was run as an induction motor and its speed varied by changing the applied d.c. voltage.

It is concluded that the qualitative behavior of the polyphase transistor-switching circuit is accurately predicted by theory. By careful determination of the many parameters in the circuit, quantitative predictions should be very precise. It is further concluded that speed control of low-power induction motors, using the switching circuit output as a power supply, is feasible, but that it is desirable to filter out the harmonic content of the switching circuit output in order to minimize undesirable losses due to the harmonics.

It is recommended that further experimental study be made, particularly with regard to speed control of induction motors, that the switching circuit design be optimized for maximum power output, that the problem of filtering the switching circuit output to remove harmonics be investigated, and that schemes for increasing the power rating of the circuit be devised.

Thesis Supervisor: Alexander Kusko

Associate Professor of
Electrical Engineering.

ACKNOWLEDGEMENTS

The authors are indebted to Professor A. Kusko, of the Electrical Engineering Department, Massachusetts Institute of Technology, for his advice and guidance as thesis supervisor; to Messrs. T. H. Putman, R. D. Thornton, and H. H. Woodson, of the Electrical Engineering Department, Massachusetts Institute of Technology, for their interest and assistance in the development of this thesis; and to Miss Catherine Ahearn, for her patience and skill in preparing the thesis in its final form.

TABLE OF CONTENTS

TABLE OF CONTENTS

TABLE OF CONTENTS

LIST OF ILLUSTRATIONS

LIST OF ILLUSTRATIONS

LIST OF ILLUSTRATIONS

SYMBOLS

a	Transistor current amplification factor
E	Applied DC voltage to converter
f	Frequency
i_b	Transistor base current
i_c	Transistor collector current
i_e	Transistor emitter current
i_a	Current in additive phase-locking loop
i_s	Current in subtractive phase-locking loop
i	Load current
$i_{d_n}^{r}$	n^{th} direct axis rotor current
$i_{q_n}^{r}$	n^{th} quadrature axis rotor current
$i_{\alpha_n}^{s}$	n^{th} α axis stator current
$i_{\beta_n}^{s}$	nth β axis stator current
I_m	Magnetizing current of core
L_s	Saturation inductance of core material
L_μ^{r}	Rotor self-inductance per phase
L_μ^{s}	Stator self-inductance per phase
L_μ^{sr}	Mutual inductance between one phase of rotor and one phase of stator
n	Order number of n^{th} harmonic
N	Number of turns on a winding
P	1. Power 2. Number of poles on motor
R	Resistance introduced into base for phase-locking

SYMBOLS

R' Inverse slope of positive-resistance portion of v-i characteristic

R_o Inverse slope of negative-resistance portion of v-i characteristic

R_o' Inverse slope of negative-resistance portion of v-i characteristic as modified by phase-locking circuit

R_L Load resistance

$R_b = r_b + r_{w_2}$ Transistor base resistance plus resistance of winding in base circuit

$R_s = r_s + r_{w_1}$ Transistor saturation resistance ($r_s \triangleq \partial V_c / \partial I_c$) plus resistance of winding in collector circuit

R^r Rotor resistance per phase

R^s Stator resistance per phase

r_{w_n} Resistance of n^{th} transformer winding

r_b Transistor base resistance

r_c Transistor collector resistance

r_e Transistor emitter resistance

r_s Transistor saturation resistance

s_m Motor slip at maximum torque

s_n Motor slip (n^{th} harmonic)

T_{em} Maximum electromagnetic torque

T_{en} Electromagnetic torque due to n^{th} harmonic in applied voltage

$\vec{V}$ Complex voltage

$\vec{V}^*$ Conjugate of complex voltage

SYMBOLS

$v_{\alpha_n}^{s}$	n^{th} harmonic of voltage applied to stator windings
$v_{\beta_n}^{s}$	n^{th} harmonic of voltage applied to stator windings
v	Load voltage
Z_L	Load impedance
Z^s	$R^s + j\omega L_\mu{}^s$
Z^r	$R^r + j\omega L_\mu{}^r$
ω	Frequency of fundamental component of applied voltage
ω_m	Motor speed
ϕ	Flux

CHAPTER 1

INTRODUCTION

With the coming of age of automation, the need for variable speed control of electric motors for use in control systems has assumed great importance. Even before automation in industry, variable speed electric motors found many applications in military servo systems. Because of the difficulty in obtaining speed control of AC motors, it has invariably been necessary to use DC motors in the aforementioned applications. This, of course, introduces the disadvantage of the commutator as well as requiring extensive additional equipment if wide speed range is desired.

There would be several advantages attendant to using induction motors in the above applications, among which are the ruggedness of the motor, the inexpensiveness of the squirrel-cage rotor induction motors, and the fact that there is no commutator. The inflexibility of the induction machine from the standpoint of speed control has prevented its wide use in control applications, but smooth speed control over any range can be provided if the line frequency is varied. Since it has not been convenient to do this in the past, the induction motor has been regarded as essentially a constant-speed machine. The switching circuit studied in this thesis offers a means of conveniently varying line frequency and, thus, varying the speed of an induction motor.

It is the purpose of this thesis to investigate analytically and experimentally the application of a switching-transistor DC to AC converter described by Royer in [1] to speed control of induction motors. This circuit has an output frequency proportional to the magnitude of the DC input voltage, so it provides the variable frequency source required to attain such speed control. Furthermore, the magnitude of the output voltage is also proportional to the DC input voltage, so the maximum torque attainable remains nearly constant since the flux density is approximately constant. By the use of phase-locking techniques described by Milnes in [2], two or more of the basic circuits may be combined to provide a polyphase power supply. Since the output of the converter is a square wave, the effect of square voltage wave excitation on the torque of an induction machine must be determined.

The operation of the basic circuit, the phase-locking principle and the effect of phase-locking on operation of the basic circuit, and the effect of applying square voltage waves to an induction machine will all be analyzed theoretically. Insofar as possible, the predictions of theory will be checked experimentally.

CHAPTER 2

PROCEDURE

In both the analytical study and the experimental work, the procedure has been to start with the simple and proceed to the more complex. For example, in the theoretical analysis, the basic circuit is first analyzed for operation with passive loads, then the phase-locking principle is studied, after which the operation of the converter with phase-locking elements included is determined. These analyses place the limits on the load which can be placed across the output and indicate the departure of operation from the ideal case. The analytical portion of the thesis is then completed with the analysis of the effect of square voltage wave excitation on the torque-speed characteristics of the polyphase induction motor.

In the experimental phase of the thesis, a similar procedure is followed. The basic single-phase converter is designed and assembled and then tested to determine operation with various passive loads. Then, successively, two-phase and three-phase circuits are assembled and tested.

The object of the experimental portion is to determine degrees of agreement with theory and practical limits of operation. Therefore, information of interest includes range of input voltage over which satisfactory operation is obtained, frequency of output for a given input voltage,

range of frequency obtainable, and power level of the output. This information is readily obtained once the circuit is properly operating.

As will be developed in the analysis of the basic circuit, the problem of starting an induction motor using the switching circuit is a difficult one. For proper operation, the circuit requires a certain minimum load impedance, and the induction motor, at starting, is almost a short circuit. Therefore, the phase of the experimental work concerned with applying the switching circuit output to the windings of an induction motor consists of trying to devise schemes for introducing impedance into the load in order to maintain oscillatory operation of the switching circuit.

The thesis follows, in general, the outline of procedure given above.

CHAPTER 3

ANALYSIS OF SWITCHING CIRCUIT OPERATION

3.1 Basic Circuit

The basic switching circuit proposed by Royer in [1] is shown in Figure I. The operation of this circuit has been described in terms of core saturation in both [1] and [2]. While such explanation does express the mode of operation of the circuit, it leaves many questions unanswered. By analyzing the circuit as a negative resistance oscillator, a more complete picture of the operation may be obtained and, in particular, the importance of the load impedance level shows up clearly.

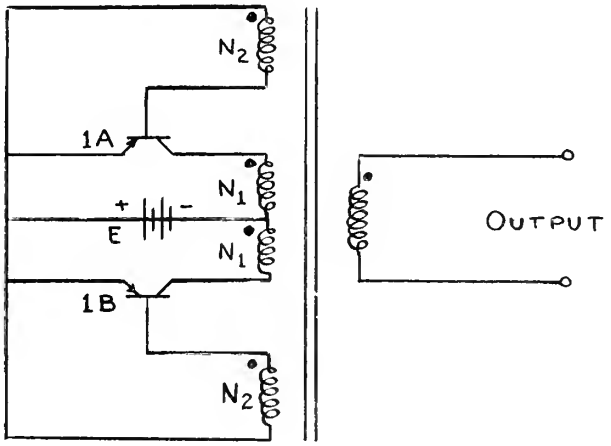

Fig. I. Basic switching circuit.

Obviously, one-half of the circuit may be investigated at a time since, when one transistor is conducting, the other is blocking and does not affect the output. The

analysis is carried out in detail in Appendix A, but the assumptions made in the analysis are important and include the following:

1. The transistors are perfect switches, i.e., when blocked the leakage current is negligible and is assumed to be zero.

2. Leakage inductances of the core windings are negligible. This assumption simplifies the analysis considerably and is justified by the fact that these inductances do not fundamentally affect circuit operation.

3. Winding resistances of the core windings may be lumped with other resistances in the circuit.

4. Based on (2) and (3), the windings may be represented as ideal transformers.

Granted these assumptions, we are able to look into the circuit of the "N_1" windings, with the magnetizing inductances and load being taken out of the circuit. The circuit may then be reduced to the form shown in Fig. II. The piecewise-linear model of the transistor is the conventional representation of a transistor in saturation.

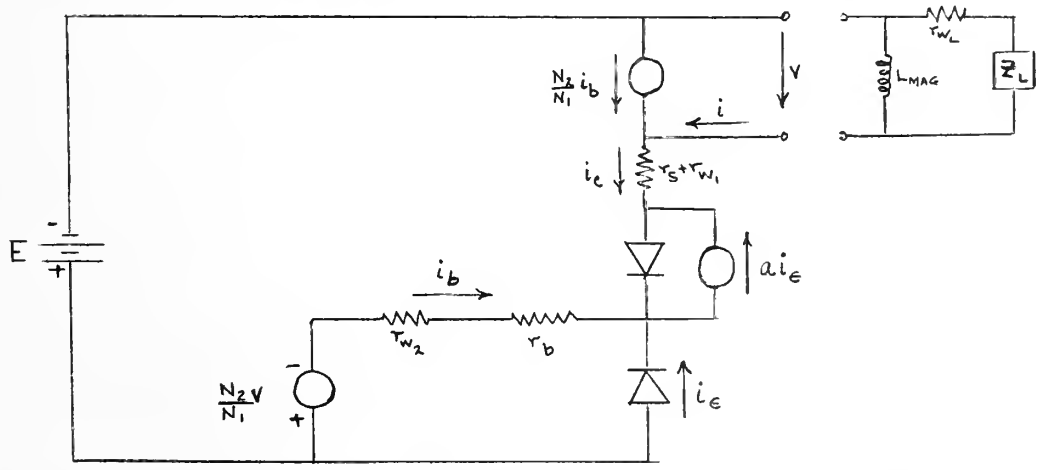

Fig. II. Representation of conducting half of switching circuit for break-point analysis.

Using conventional methods of break-point analysis, the v-i characteristic of the circuit can be determined. Then, from symmetry considerations, the picture may be completed by adding the effect of the other half of the circuit, the resultant v-i characteristic being shown in Fig. III. The quantities of interest are as follows:

$$V_o = \frac{E}{1 + \frac{1}{nR_b}\left(\frac{aR_s}{1-a}\right)} \tag{1}$$

$$I_o = V_o \left[\frac{1 - a(n+1)}{n^2(1-a)R_s}\right] \tag{2}$$

$$R_o = \frac{n^2(1-a)R_b}{1 - a(n+1)} \tag{3}$$

$$R' = \frac{R_s(n^2R_b)}{R_s + n^2R_b} \tag{4}$$

where

$$R_b = r_b + r_{w2} \tag{5}$$

$$R_S = r_s + r_{w1} \tag{6}$$

$$n = N_1/N_2 \tag{7}$$

Note that R_o is negative for any normal value of the turns ratio, so that the circuit, as seen from the magnetizing inductance of the core, displays the volt-ampere characteristic of a negative-resistance oscillator.

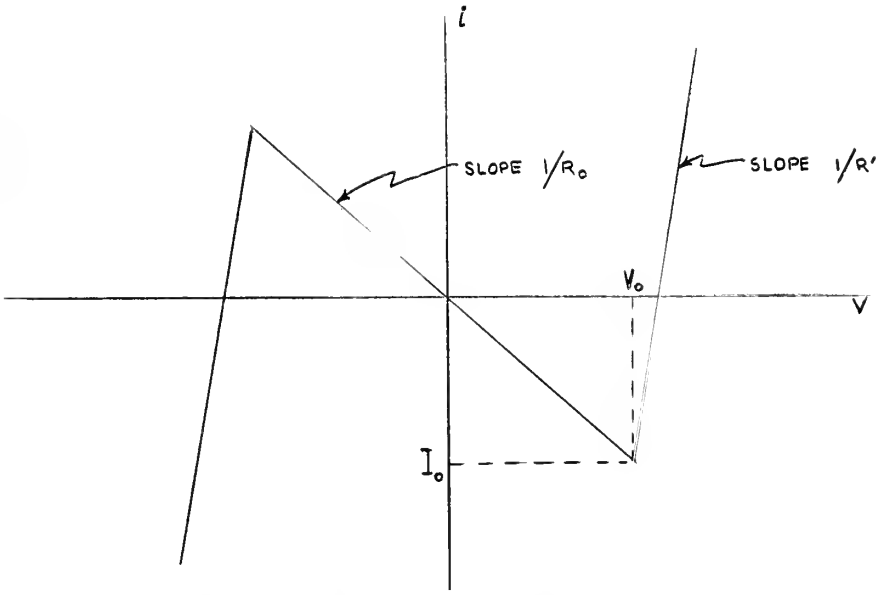

Fig. III. v-i characteristic of switching circuit as viewed from magnetizing inductance of core.

3.2 Effect of Load on Basic Circuit v-i Characteristic

Based on the foregoing, the circuit may be represented by the magnetizing inductance and the load placed across the terminals of a black box whose v-i characteristic is known. This representation is shown in Fig. IV.

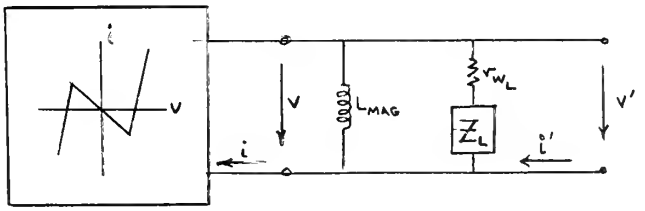

Fig. IV. Representation of switching circuit and load.

For the moment, assume that the magnetizing inductance is infinite and that the load is resistive. Then if we lump the winding resistance of the load and the load itself and call the resultant resistance R_L, we can look in at the

v'-i' terminals and observe the effect of R_L on circuit operation. As shown in Fig. V, the effect of the load is to change the value of the negative resistance. The

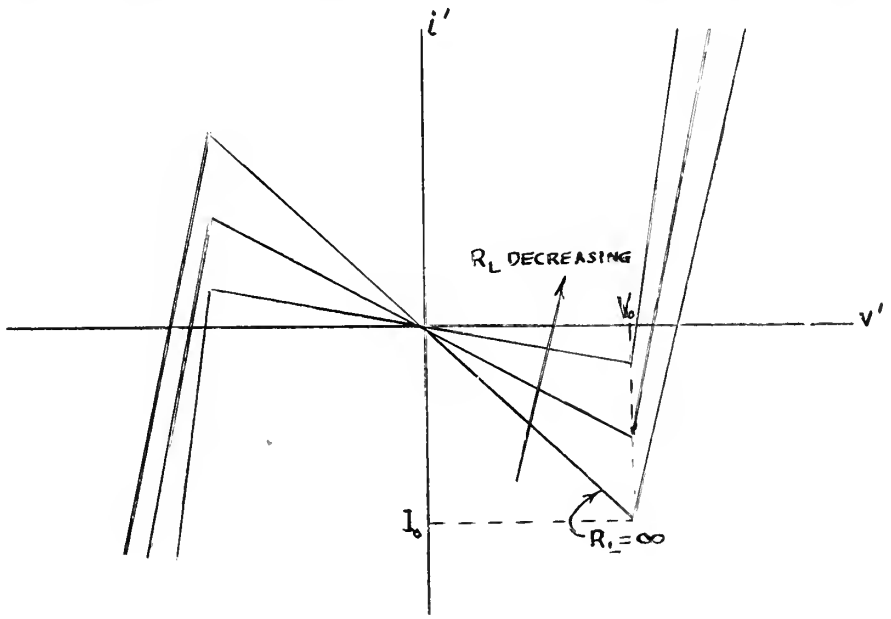

Fig. V. v'-i' characteristics of load and negative resistance oscillator, showing the effect of R_L on operation.

practical importance of this is obvious in that if R_L equals R_o (R_o being defined by Equation (3)), the circuit no longer looks like a negative resistance, so oscillatory behavior will not occur. This poses a difficult problem to the purpose of this thesis for it is hoped to apply the output of this circuit to the stator windings of an induction motor. Since, at starting, the resistance of an induction motor is very nearly zero, the effect of placing this motor directly across the switching circuit output may be to stop the oscillations of that circuit.

Therefore, at starting, some means will have to be devised to make the load present a high impedance to the switching circuit.

3.3 Oscillatory Behavior of the Basic Circuit

It has so far been shown that the basic circuit displays a negative resistance portion in its volt-ampere characteristic, and it has been implied that this can lead to oscillatory behavior. This effect will now be shown.

When we look into the N_1 windings of the basic circuit from the magnetizing inductance of the core, we see the v-i characteristic shown in Fig. VI(a). For simplicity, the case

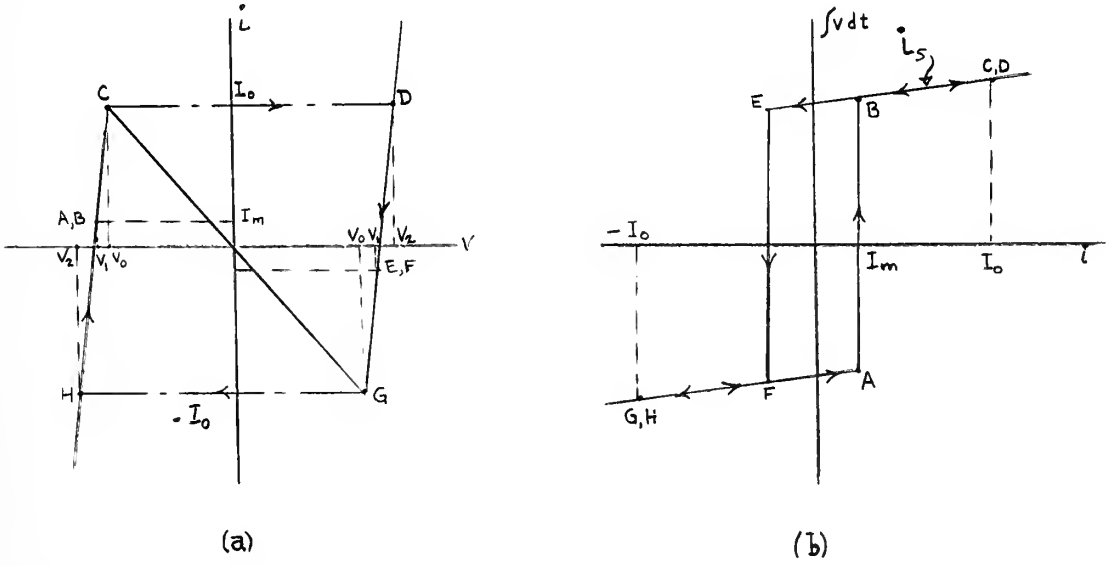

Fig. VI. (a) v-i characteristic of switching circuit.
(b) Typical hysteresis loop for core material.
Letters refer to particular states in the operation.

where R_L is infinite is shown. If some finite value of R_L is taken (so long as R_L is greater in magnitude than R_o), the

only effect is to change the slopes of the v-i characteristic; the principle remains the same.

Suppose that the initial state of the core is at point A in Fig. VI(b). On the v-i curve in Fig. VI(a), this point is located as shown. So there is some voltage, V_1, across the windings and a magnetizing current, I_m, flowing in the windings. So far as the v-i curve is concerned, this state remains while the core absorbs $2\lambda_s = 2N\phi_s$ volt seconds. After this absorption, the core is at point B, as indicated in Fig. VI(b). So far as the v-i curve is concerned points A and B are identical.

At point B, the core saturates and the voltage and current are constrained to operate on the v-i characteristic and are related by

$$v = L_s \frac{di}{dt} \tag{8}$$

so the current and voltage increase (voltage becomes less negative) along the path BC, indicated in Fig. VI(a). At point C on the v-i curve, the current cannot continue to increase in accordance with Equation (8) because the v-i locus will not allow it. So, still referring to Fig. VI(a), operation switches almost instantaneously to point D. (The time interval here depends upon the switching time of the transistor.) At point D, the v-i locus is such that the relationship given in Equation (8) may again be satisfied, so both current and voltage decrease until point E on the hysteresis loop is reached, at which time the core desaturates.

Voltages and currents then remain constant while the core once more absorbs $2\lambda_s$ volt seconds. At that point, saturation again occurs and the same sort of operation as is described above is repeated to close the oscillation loop.

Looked at as a function of time the voltages and currents appear as shown in Fig. VII. If the saturation

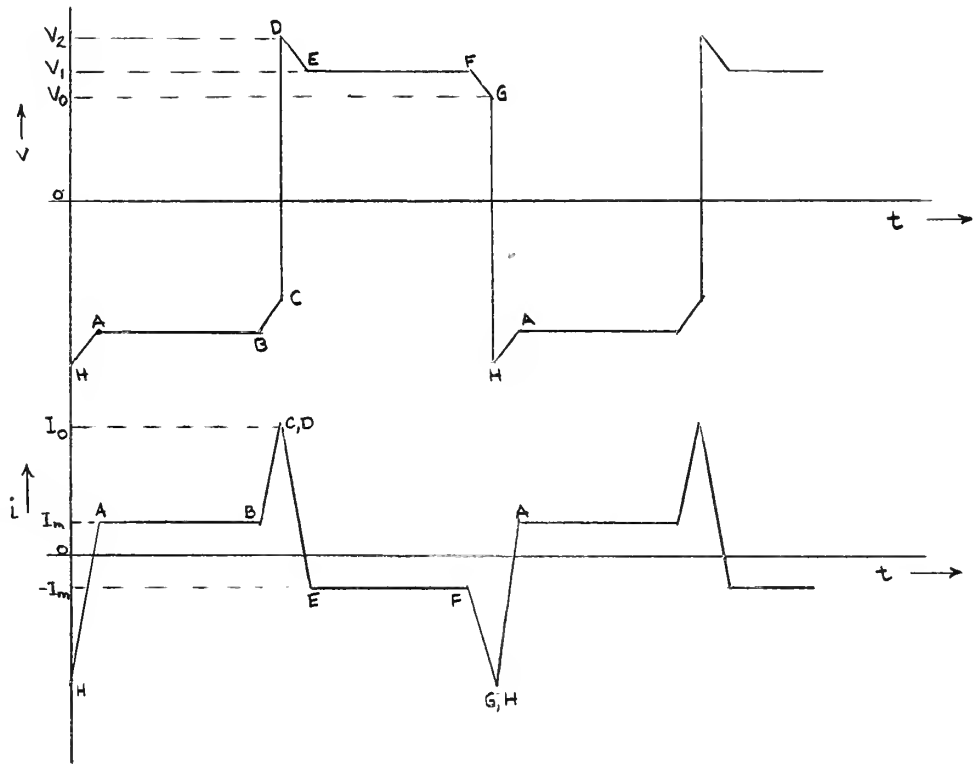

Fig. VII. Current and voltage waveforms in steady state operation of switching transistor circuit.

inductance were zero and if the transistors switched instantaneously, the transition from B to E and F to A would be instantaneous and a perfect square wave output would be obtained. Furthermore, the frequency of operation would depend solely on the time it takes for the core to go

from negative to positive saturation, i.e.,

$$2\lambda_s = V_1 \Delta t \tag{9}$$

where Δt is the time for one half cycle to occur. Then, we have

$$f = \frac{V_1}{4N_1\Phi_s} \tag{10}$$

which is the fundamental frequency relationship for this circuit.

One interesting fact is immediately evident. In the usual approach to analyzing the operation of this circuit, the frequency relationship has been written with E replacing V_1 in Equation (10). Neglecting other time intervals in the cycle (i.e. assuming L_s is zero and transistor switches instantaneously), for any non-zero value of R_s, the ideal frequency is approached more and more closely as n^2R_b is made very much larger than R_s. This is shown by the following equation:

$$V_1 = (E - I_m R_s) \frac{n^2 R_b}{R_s + n^2 R_b} \tag{11}$$

Since $I_m R_s$ is very much smaller than E, it can be neglected, so the importance of the n^2R_b term in determining the deviation of the frequency from that predicted for the ideal case is evident. Unfortunately, as can be seen by reference to Equation (3), an increase in the quantity n^2R_b also increases R_o, thus increasing the minimum allowable load impedance.

Insofar as operation of the basic circuit is concerned, the only other question of importance concerns the relative

magnitudes of the various time intervals in determining frequency.

3.4 Importance of Various Time Intervals in Determining Frequency

Reference to Fig. VII shows that two parasitic time intervals exist in any given cycle, that is, the time to go from B to C and from D to E, and the switching time of the transistor (C to D). We can find the time to go from D to G to account for the intervals from B to C and D to E, and the switching time of the transistor may be estimated using the high-frequency equivalent circuit.

To determine the time involved in going from D to G, we can use Equation (8) and the following relationship:

$$v = \left(\frac{R_s n^2 R_b}{R_s + n^2 R_b}\right) i + \frac{E n^2 R_b}{R_s + n^2 R_b} \qquad (12)$$

This calculation is made in Appendix B, using representative values of the circuit parameters, and shows that the time interval involved in one complete cycle is approximately twenty-five micro-seconds.

In order to estimate the switching time of the transistor, the high-frequency piecewise-linear model of the transistor given in [4] is used. Again calculations are included in Appendix B and show that the switching time of the transistor is of the order of micro-seconds, so the time interval for switching the transistors is negligible.

When we consider the fact that the maximum frequency we are interested in for our purposes is 100 cps, we see

that the minimum period we will be dealing with is ten milliseconds; therefore, neither of the parasitic time intervals is of any consequence in determining the frequency of operation of the oscillator.

3.5 Conclusions Concerning Operation of the Basic Circuit

Based on the foregoing, the following important conclusions can be made with regard to operation of the single phase switching-transistor circuit:

1. There is a minimum value of load impedance, below which oscillatory behavior of the switching circuit ceases.

2. Because of the aforementioned restriction on the value of load impedance, the power which can be delivered to the load is limited. (Since $P = V_{Load}^2/R_L$.)

3. The frequency of operation approaches more closely the ideal predicted frequency as the quantity n^2R_b is increased. Unfortunately, increasing n^2R_b has the concomitant effect of increasing the minimum allowable load impedance.

4. Parasitic time intervals are of no consequence in determining frequency of operation of the circuit over the range in which we are interested.

The next step is to investigate the phase-locking principle and determine the effect of phase-locking on the operation of the basic circuit.

CHAPTER 4

POLYPHASE SWITCHING CIRCUITS

4.1 Phase-locking Principle

By utilizing phase-locking techniques proposed by Milnes in [2], two or more of the converters described in Chapter 3 may be locked together with their output differing in phase by any desired amount. In this chapter, a circuit in which two of the basic converters are locked together with a 120° phase difference will be described. In order to construct a three-phase system, it is then simply necessary to add another converter locked 120° behind the other two.

In order to link the basic converters to form polyphase systems, the arrangement shown in Fig. VIII is used. In this arrangement, the elements designated L_1 and L_2 are saturable reactors, the volt-time ratings of which are adjusted to provide the desired phase difference between the outputs, V_1 and V_2.

The analysis of the basic converter circuit as a negative-resistance device led to many interesting conclusions with regard to its operation, particularly giving an insight into the effect of various circuit parameters on operation. In analyzing the phase-locking principle, this technique is not useful. Instead, operation is conveniently investigated in terms of volt-time areas.

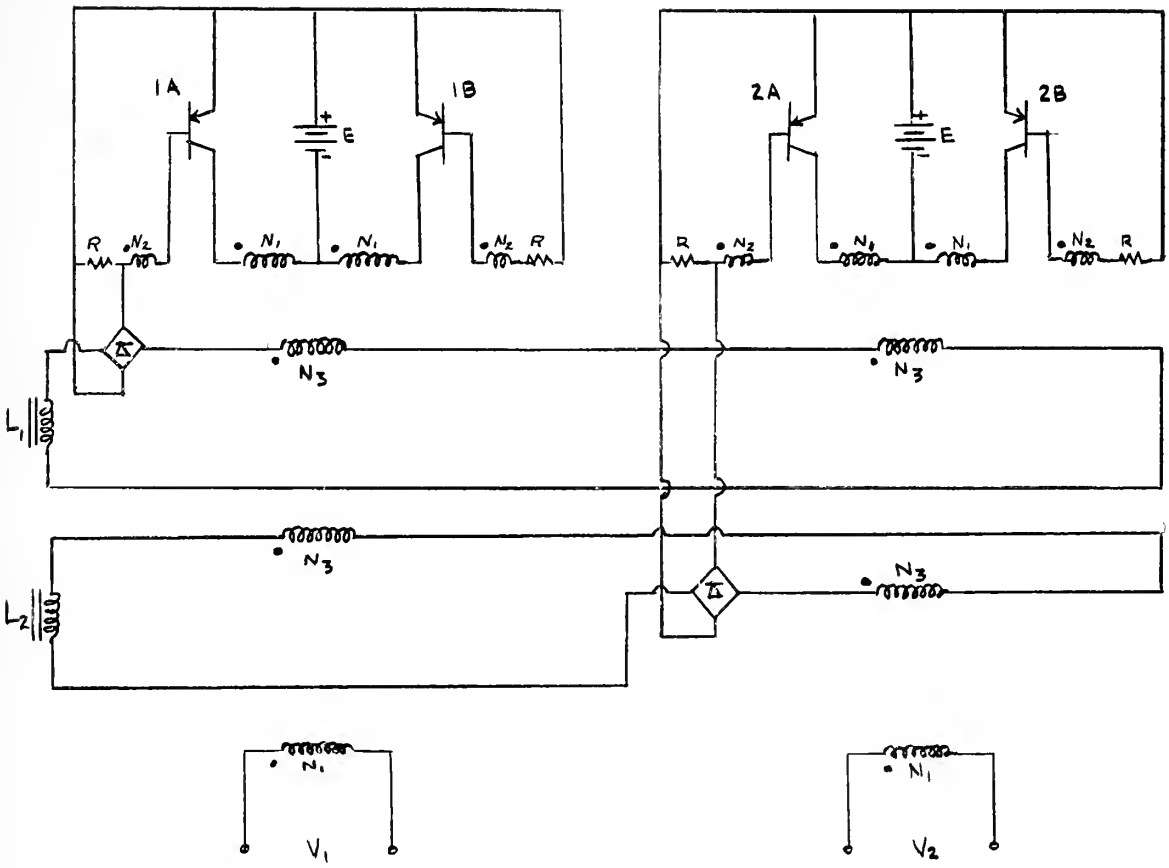

Converter No. 1 Converter No. 2

Fig. VIII. Arrangement for locking two converters together with predetermined phase shift between the outputs.

The desired output waveforms are shown in Fig. IX(a) and (b). Now, reference to Fig. VIII shows that, with winding polarities as indicated, $(V_1+V_2)\ N_3/N_1$ appears across L_1 and $(V_1-V_2)\ N_3/N_1$ appears across L_2. These sum and difference voltages are shown in Fig. IX (c) and (d).

Fig. IX (c) and (d) show that for the phase difference desired, the volt-time rating of L_2 must be twice that of L_1. It is now desired to relate the volt-time ratings of the

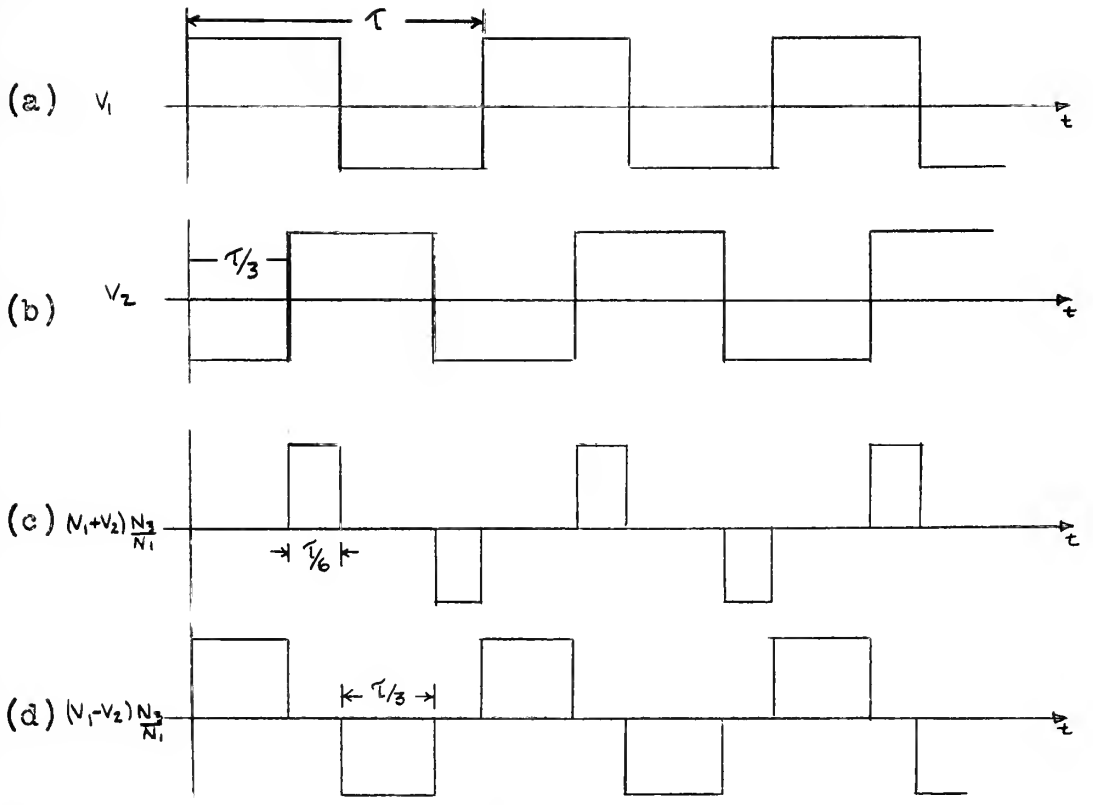

Fig. IX. Output voltages from two-phase circuit and sum and difference voltages which appear across saturable reactors.

saturable reactors to that of the main windings. First, we recognize that in any half cycle each of the saturable reactors goes from negative saturation to positive saturation. Then we can say that in one half-cycle, L_1 absorbs:

$$2V_1 \frac{N_3}{N_1} \frac{\tau}{6} \quad \text{volt secs.} \tag{13}$$

and L_2 absorbs:

$$2V_1 \frac{N_3}{N_1} \frac{\tau}{3} \quad \text{volt secs.} \tag{14}$$

In this half-cycle, the main windings absorb:

$$V_1 \frac{\tau}{2} = 2N_1\phi_s \text{ volt secs.} \tag{15}$$

from which we can solve for T.

We then observe that L_1 and L_2 together absorb:

$$V_1 \frac{N_3}{N_1} \tau = 2N_{L_1}\phi_{L_1} + 2N_{L_1}\phi_{L_2} \quad \text{volt secs.} \tag{16}$$

where ϕ_{L_1} and ϕ_{L_2} are the saturation fluxes of L_1 and L_2, respectively.

Then, using the fact that the volt-time rating of L_2 must be twice that of L_1, and assuming that ϕ_{L_1} equals ϕ_{L_2} (as it will in the practical case), we find that:

$$N_{L_1}\phi_L = \frac{2}{3} N_3 \phi_S \tag{17}$$

and

$$N_{L_2}\phi_L = \frac{4}{3} N_3 \phi_S \tag{18}$$

Equations (17) and (18) are the fundamental relationship between the volt-time ratings of the saturable reactors and the volt-time ratings of the phase-locking circuit turns (N_3) on the main cores when two converters are locked together with 120° phase shift.

How does this assure the desired phase-locking? If the outputs are not out of phase by 120°, the sum and difference voltages will be different from those shown in Fig. IX. For example, if the outputs are out of phase by less than 120°, the sum $(V_1+V_2)\ N_3/N_1$ will appear across L_1 earlier than is shown in Figure IX (c). However, L_1 is designed to absorb a certain number of volt-seconds, so, after absorbing this designed amount, it will saturate. The sum voltage will then

appear across the rectifier bridge, thence across the resistance in the base circuit of transistor 1A in such a direction as to make the transistor non-conducting. (Refer to Fig. VIII.) Thus, the transistor will switch sooner than it would have without phase-locking. By following cycles of this sort the two circuits finally arrive at the desired phase relationship. A more detailed discussion of the above action for a quadrature phase-locking circuit is given in [2]. It should be mentioned that investigation of the phase-locking action in detail shows that the relationships given in Equations (17) and (18) are not exact in the practical case, but that the volt-time ratings of the saturable reactors should be slightly less than those ideal values [2]. The discrepancy is small and is not amenable to precise prediction, so in designing the circuit it is desirable to provide taps on the windings on L_1 and L_2 in order to permit adjustment of the number of turns to give exactly the desired phase shift.

4.2 Effect of Phase-locking on Operation of Switching Circuit

In this section we are interested in determining the effect of introducing phase-locking on the operation of the basic circuit. That is to say, how does it affect the converter operating as a negative-resistance oscillator?

The analysis is made in detail in Appendix C. In order to simplify the equations, the two-phase circuit is analyzed, extension to the three-phase case being made by deduction. In order to make this analysis it is necessary

to regard all transformers in the circuit as ideal except for winding resistance. Accordingly, self-inductances of the windings are assumed to be zero and magnetizing inductances are assumed to be infinite.

As shown in Appendix C, the basic effect in the steady state of adding the phase-locking circuit is to modify the v-i characteristic as seen from the load. The slope of the negative resistance portion (R_o in Fig. III) is changed in accordance with the following relation:

$$R_o' = \frac{R_o(R+R_b)}{R_b(1+K)} \tag{19}$$

where R_b is as defined in Equation (5), R_o is defined in Equation (3), R is the resistance introduced into the base circuit of each of the transistors (See Fig. VIII), and K is defined by the following:

$$K \approx \frac{n I_m\left[n(1-a)(R+R_b)+aR_s\right]}{\left[E+\left(\frac{a}{1-a}\right)\left(\frac{RR_s}{R+R_b}\right)I_m\right]\left[1-a(n+1)\right]}\left[\frac{N_3}{N_1}-\frac{\left[1-a(n+1)\right]R}{n(1-a)(R+R_b)}\right] \tag{20}$$

where I_m is the magnetizing current of the main core (for example, see Fig. VI(b)) and other quantities have been previously defined. The magnitude of K is normally small but, whatever its magnitude, the effect is to make R_o' larger.

Therefore, the most important result of introducing phase-locking in the two-phase case is to increase the value of the negative-resistance portion of the v-i characteristic as seen from the load, thus increasing the minimum allowable load impedance for oscillatory operation.

In the three-phase case, the effect is even more pronounced in that the center converter sees more additional resistance because of the additional phase-locking windings so that the quantity, K, in Equation (19) will be further increased, thus increasing R_o' once more.

These effects are all observed experimentally. Each time the number of phases is increased in going from single-phase to three-phase operation, it is found necessary to increase the minimum load resistance to sustain oscillatory operation.

CHAPTER 5

DESIGN OF THREE-PHASE SWITCHING-TRANSISTOR CONVERTERS

5.1 The Three-phase Circuit

As is mentioned in Section 4.1, the three-phase switching-transistor circuit is made up of three converters, each differing in phase from the others by 120°. Such an arrangement is shown in Fig. X. In this scheme, the volt-time ratings of L_1 and L_3 are equal, as are those of L_2 and L_4. The volt-time rating of L_2 and L_4 is twice that of L_1 and L_2. In actual practice, the converters are supplied from the same D.C. source, three different sources being shown in Fig. X in order to simplify the diagram.

The design of the particular circuit used in experimental work for this thesis is outlined in Appendix E, the following procedure being given for the general case.

5.2 Determination of Number of Turns on Cores

The first step is to determine the number of turns to be used in the various windings shown in Fig. X. For design purposes, the frequency relationship given in Equation (10) may be approximated by the ideal relationship which follows:

$$f = \frac{E}{4 N_1 \Phi_s} \tag{21}$$

In order to solve for N_1, three quantities, f, E, and Φ_s, are required. Φ_s is a function of the core material and dimensions and is assumed known. For a constant frequency

Fig. X.

Three-phase Switching Circuit.

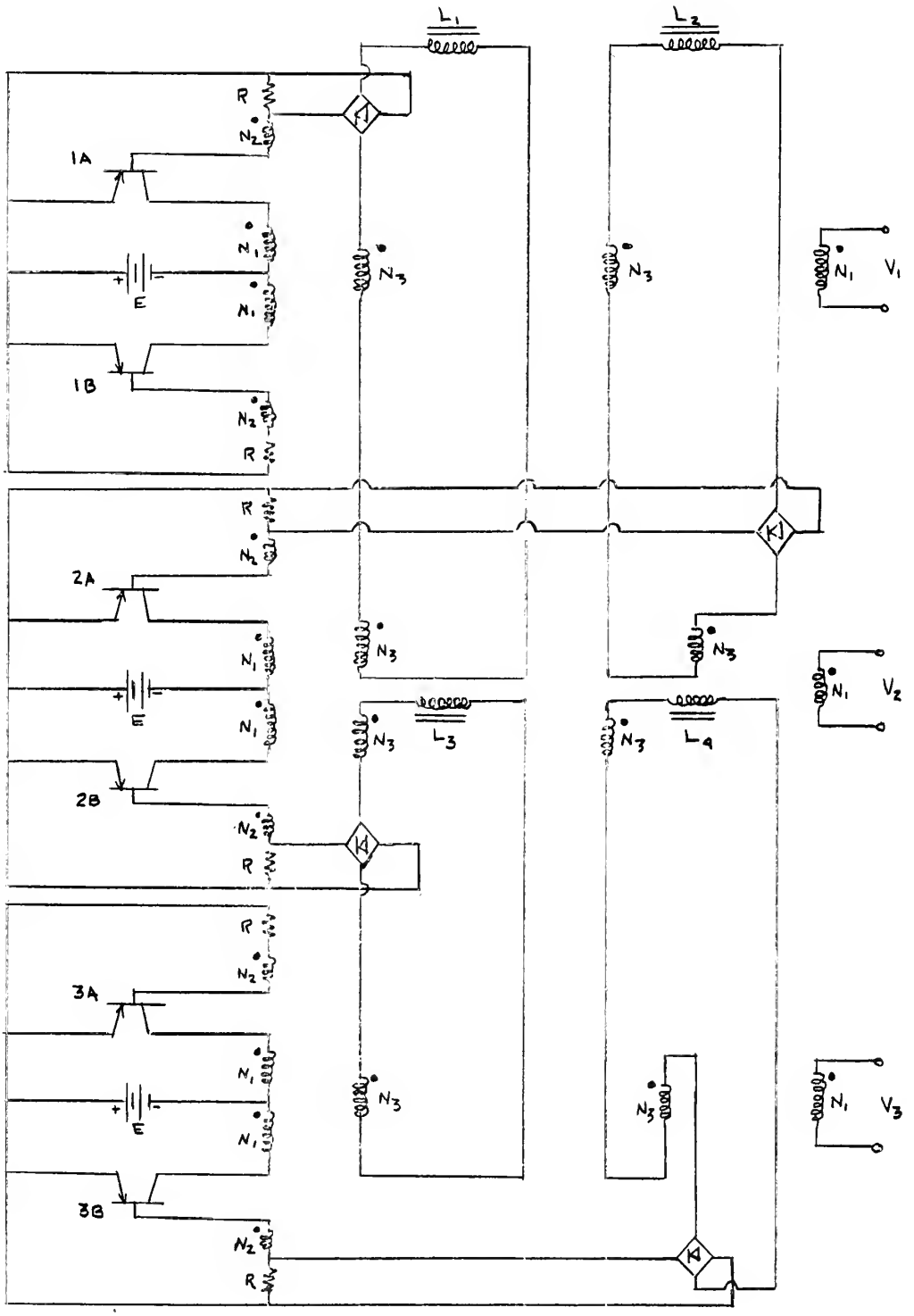

circuit, f is known uniquely. In the variable frequency case, it is the maximum frequency at which the converter is desired to operate. The input voltage, E, is dependent upon collector characteristics of the transistor operating in the common emitter configuration and upon the maximum allowable collector-to-emitter voltage for the transistor. This last characteristic gives the maximum allowable value of input voltage. In this connection, it must be remembered that when the transistor is cut off, twice the input voltage appears across collector-to-emitter, so the maximum permissible input voltage is one-half the maximum allowable collector-to-emitter voltage.

Knowing all these quantities, N_1 may be calculated. If it is important that the maximum frequency of operation be achieved, the calculation should be for some input voltage less than the maximum allowable since, as was shown in Section 3.3, the voltage which appears across the core is less than E.

N_2 is determined by the amount of base current required to saturate the transistor. Referring to typical collector characteristics for the transistor in the common emitter configuration, as shown in Fig. XI, a load line for the maximum allowable voltage is chosen so as to obtain the maximum possible power from the transistor when saturated. For the present, assume that this load line is as shown. It can be seen that in order to saturate the transistor (I_c = 400 ma), the base current must be about 10 ma. Then, knowing the value of the resistances in the base, the voltage required across

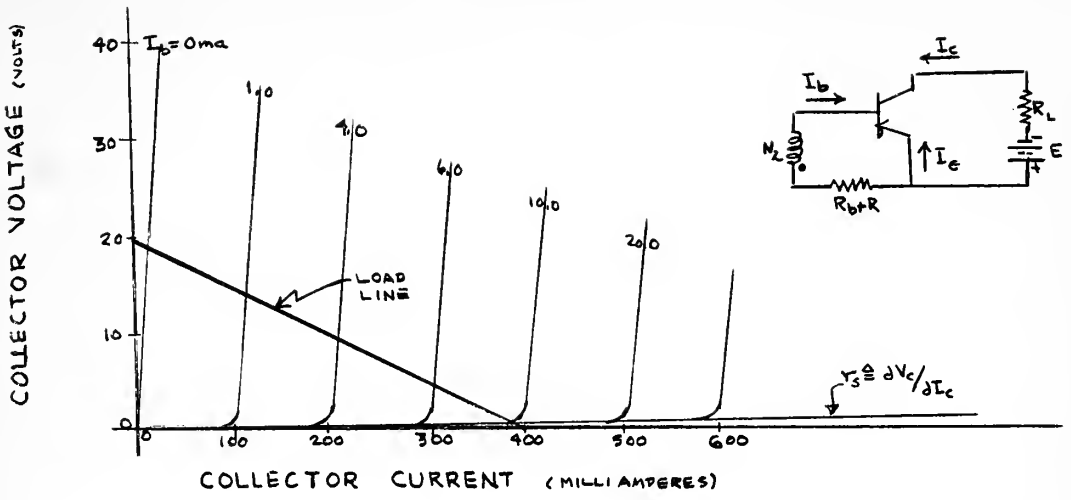

Fig. XI. Typical collector characteristics for power transistor in common emitter configuration.

the "N_2" winding to give this required base current may be determined. Knowing this, the turns ratio, N_2/N_1, may be found for the maximum input voltage. In the practical case, N_2 may be chosen larger than the value indicated by the above to provide a safety factor and assure saturation. It must be recognized, however, that this will increase dissipation in the base.

There is no particular requirement on the value of N_3 except that when the phase-locking saturable reactors do saturate, the voltage which appears across R in the base circuit of the transistor (see Fig. X) must be sufficient to overcome the voltage across N_2 and block the transistor. Therefore, it should be sufficient to make N_3 equal to N_2. It should be mentioned that it is desirable to make N_3 as small as possible in order to limit winding resistance losses and to reduce the total number of turns on a core.

Having chosen a value of N_3, the required number of turns on the phase-locking saturable reactors may be determined from Equations (17) and (18).

Based upon the above, the number of turns in all the windings indicated in Fig. X may be determined. Another important factor in this design is the determination of the load line shown in Fig. XI.

5.3 Determination of Load Line for Maximum Power Output

In this discussion, the circuit shown in Fig. XII will be investigated. Essentially, this is what we would like the

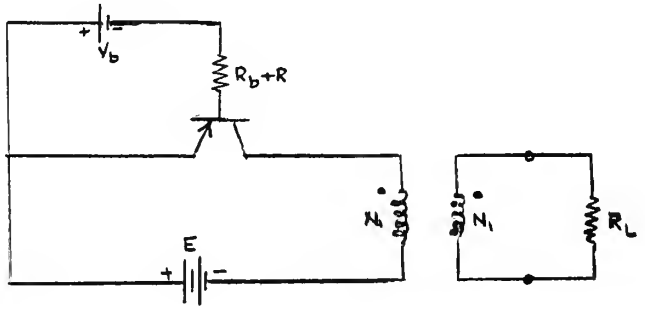

Fig. XII. Transistor in common-emitter configuration.

basic converter circuit to reduce to when the transistor is saturated. (This presumes that V_b is chosen to give this condition.) Then, provided there were no other limitation on the value of load impedance, R_L would be chosen in order that the maximum power would be delivered to the load, that is, so that the transistor is delivering all the power it can without exceeding the maximum current rating. It should be noted that the circuit used in experimental work in connection with this thesis was designed on this basis.

However, as was shown in Section 3.2, the choice of R_L is not an independent one in this switching circuit, for it must be larger in magnitude than the negative resistance portion of the v-i characteristic of the circuit. Therefore, if the maximum amount of power is to be delivered to the load, R_o must be minimized. Reference to Equation (3) (Equation (19) for the polyphase case), shows that R_o is a function of the collector-to-base transformer turns ratio, the total resistance in the base circuit, and the current amplification factor of the transistor. Of interest is the ability of the designer to minimize R_o by controlling the values of the first two of these factors. With regard to the turns ratio, n, we have:

$$\frac{\partial R_o}{\partial n} = \frac{[1-\alpha(n+1)]\,[2n R_b(1-\alpha)] - [n^2 R_b(1-\alpha)][-\alpha]}{[1-\alpha(n+1)]^2} \tag{22}$$

Equating this to zero and solving for n, we find:

$$n \triangleq \frac{N_1}{N_2} = \frac{2(1-\alpha)}{\alpha} \tag{23}$$

in which case

$$R_{o_{min}} = \frac{-4(1-\alpha)^2 R_b}{\alpha^2} \tag{24}$$

But this result requires that N_2 be greater than N_1, which is totally unrealistic. Therefore, it is concluded that the best the designer can do, in choosing this turns ratio to reduce the value of R_o, is to make n as small as possible consistent with acceptable amounts of dissipation in the base circuit.

The primary means of minimizing R_o is, then, to reduce the value of total resistance in the base. This resistance is comprised of the transistor base resistance, the winding resistance in the base, and the external resistance, R, introduced into the base in the phase-locking circuit (Refer to Fig. X). By proper design of the core windings, the second may be made very small. The external resistance, R, is also small, so the most important resistance in the base circuit is the non-controllable base resistance of the transistor itself.

The problem reduces to minimizing all resistances in the circuit by careful design of the core windings and by introducing the smallest possible resistance into the base for phase-locking. Then, by judicious choice of the turns ratio, n, the magnitude of R_o may be controlled. It must be remembered, however, that there is a limit on the value of turns ratio below which dissipation in the base becomes undesirably large. This dissipation, besides representing a loss of power, also results in internal heating of the transistor.

No simple rule can be given for determining the load line for maximum power output since so many factors enter into the problem. However, the principles outlined above do give the designer a point of departure.

CHAPTER 6

OPERATION OF INDUCTION MOTOR EXCITED BY POLYPHASE SWITCHING CIRCUIT OUTPUT

6.1 Technique of Analysis

In the analysis which follows, an idealized model of the rotating electrical machine will be used and constraints will be applied to make it operate as an induction motor. The techniques employed are those developed in the course in Electric Power Modulators (6.06) given at Massachusetts Institute of Technology. The analysis will be made of a two-phase machine since the results are perfectly general and can be applied to the three-phase case by making a symmetrical component transformation.

The following assumptions are made with regard to the machine:

1. Rotor and stator are non-salient, i.e., the air gap is uniform.
2. The stator windings are symmetrical and sinusoidally distributed in space quadrature.
3. The permeability of the iron is infinite.
4. Slot effects may be neglected.

6.2 Equations Describing Machine

From [5] we have the following relations for the generalized electromechanical power modulator:

$$\begin{bmatrix} v_a^s \\ v_b^s \\ v_a^r \\ v_b^r \end{bmatrix} = \begin{bmatrix} R^s + pL_\mu^s & 0 & pL_\mu^{sr}\cos\phi & -pL_\mu^{sr}\sin\phi \\ 0 & R^s + pL_\mu^s & pL_\mu^{sr}\sin\phi & pL_\mu^{sr}\cos\phi \\ pL_\mu^{sr}\cos\phi & pL_\mu^{sr}\sin\phi & R^r + pL_\mu^r & 0 \\ -pL_\mu^{sr}\sin\phi & pL_\mu^{sr}\cos\phi & 0 & R^r + pL_\mu^r \end{bmatrix} \times \begin{bmatrix} i_a^s \\ i_b^s \\ i_a^r \\ i_b^r \end{bmatrix} \qquad (25)$$

$$T_e = L_\mu^{sr}\left[(i_a^r i_b^s - i_b^r i_a^s)\cos\phi - (i_a^r i_a^s + i_b^r i_b^s)\sin\phi\right] \qquad (26)$$

where the currents and voltages are measured on the fixed stator and moving rotor. In discussing the induction motor, it is more convenient to represent the rotor currents and voltages which are moving in space by equivalent quantities which are stationary with respect to the stator. To do this, the α-β, d-q transformation is employed:

$$\begin{bmatrix} X_\alpha^s \\ X_\beta^s \\ X_d^r \\ X_q^r \end{bmatrix} = \begin{bmatrix} 1 & 0 & 0 & 0 \\ 0 & 1 & 0 & 0 \\ 0 & 0 & \cos\phi & -\sin\phi \\ 0 & 0 & \sin\phi & \cos\phi \end{bmatrix} \times \begin{bmatrix} X_a^s \\ X_b^s \\ X_a^r \\ X_b^r \end{bmatrix} \qquad (27)$$

Applying this transformation to Equations (25) and (26), the following are obtained:

$$\begin{bmatrix} v_\alpha^s \\ v_\beta^s \\ v_d^r \\ v_q^r \end{bmatrix} = \begin{bmatrix} R^s + pL_\mu^s & 0 & L_\mu^{sr}p & 0 \\ 0 & R^s + pL_\mu^s & 0 & L_\mu^{sr}p \\ L_\mu^{sr}p & L_\mu^{sr}\dot{\phi} & R^r + pL_\mu^r & L_\mu^r\dot{\phi} \\ -L_\mu^{sr}\dot{\phi} & L_\mu^{sr}p & -L_\mu^r\dot{\phi} & R^r + pL_\mu^r \end{bmatrix} \times \begin{bmatrix} i_\alpha^s \\ i_\beta^s \\ i_d^r \\ i_q^r \end{bmatrix} \qquad (28)$$

and

$$T_e = \frac{P}{2} L_\mu^{sr}\left[-i_\alpha^s i_q^r + i_\beta^s i_d^r\right] \qquad (29)$$

By applying various constraints to Equation (28), the performance of the induction motor may be studied for any conditions of interest. In this thesis, we are interested in the effect of varying line frequency and voltage on maximum torque and in the effect of harmonic content in the applied voltage on the torque-speed characteristics, as well as the

effect of these harmonics on heat generation in the machine. These factors are all studied in the following sections.

6.3 Effect of Harmonic Content in Applied Voltage on Torque

In previous analyses [5], the voltage applied to the stator windings of an induction machine has been represented by a single sinusoid. Since the object of this thesis is to apply the output of the polyphase switching circuit to the stator windings, the effect of such excitation on the torque-speed characteristics of the machine must be determined. Furthermore, the effect of this excitation on machine heating may be important. This last will be discussed in the following section.

For the case of balanced two-phase excitation, the stator excitation voltages may be represented by the following:

$$v_\alpha^s = \frac{4V}{\pi} \sum_{\substack{n=1 \\ n \text{ odd}}}^{\infty} -\frac{(j)^{n+1}}{n} \mathcal{R}e\left(\epsilon^{jn\omega t}\right) \tag{30}$$

$$v_\beta^s = \frac{4V}{\pi} \sum_{\substack{n=1 \\ n \text{ odd}}}^{\infty} \frac{-(j)^{n+1}}{n} \mathcal{R}e\left(\epsilon^{jn\omega t - n\pi/2}\right) \tag{31}$$

where 2V is the peak to peak magnitude of the applied square wave. If we then define the following complex quantities:

$$\vec{V}_{\alpha_n}{}^s \triangleq \frac{-(j)^{n+1}}{n} \frac{4V}{\pi} \tag{32}$$

$$\vec{V}_{\beta_n}{}^s \triangleq \frac{-(j)^{n+1}}{n} \frac{4V\epsilon^{-jn\pi/2}}{\pi} \tag{33}$$

we can write

$$v_\alpha^s = \sum_{\substack{n=1 \\ n\ odd}}^{\infty} \mathcal{R}e \left[\vec{V}_{\alpha_n}^{\,s} \epsilon^{jn\omega t} \right] \tag{34}$$

$$v_\beta^s = \sum_{\substack{n=1 \\ n\ odd}}^{\infty} \mathcal{R}e \left[\vec{V}_{\beta_n}^{\,s} \epsilon^{jn\omega t} \right] \tag{35}$$

Note that:

$$\vec{V}_{\beta_n}^{\,s} = (-j)^n \vec{V}_{\alpha_n}^{\,s} \tag{36}$$

Now we recognize that in an induction motor the rotor windings are shorted so that V_d^r and V_q^r are constrained to be zero, so all the voltage constraints on Equation (28) are known.

In order to solve Equations (28) and (29), it is assumed that mechanical transients are very long compared to electrical transients. Therefore, the aforementioned equations may be solved for any desired steady-state value of mechanical speed of rotation. Furthermore, in the steady-state with sinusoidal excitation, the operator "p" in Equation (28) may be replaced by $j\omega$, providing the voltages and currents are represented in their complex forms.

Since the applied voltage is comprised of an infinite series of sinusoids, the effect of all must be included. The substitutions mentioned in the preceding paragraph convert Equation (28) to a set of linear differential equations with constant coefficients, so superposition applies. Therefore, we solve for the n^{th} component in the steady state and obtain the general result by summing n components, where n goes from

one to infinity. Subject to these conditions, Equation (28) becomes:

$$\begin{bmatrix} \vec{V}_{\alpha_n}^{\,s} \\ \vec{V}_{\beta_n}^{\,s} \\ 0 \\ 0 \end{bmatrix} = \begin{bmatrix} R^s+jn\omega L_\mu{}^s & 0 & jn\omega L_\mu{}^{sr} & 0 \\ 0 & R^s+jn\omega L_\mu{}^s & 0 & jn\omega L_\mu{}^{sr} \\ jn\omega L_\mu{}^{sr} & \omega_m L_\mu{}^{sr} & R^r+jn\omega L_\mu{}^r & \omega_m L_\mu{}^r \\ -\omega_m L_\mu{}^{sr} & jn\omega L_\mu{}^{sr} & -\omega_m L_\mu{}^r & R^r+jn\omega L_\mu{}^r \end{bmatrix} \times \begin{bmatrix} I_{\alpha_n}^{\,s} \\ I_{\beta_n}^{\,s} \\ I_{d_n}^{\,r} \\ I_{q_n}^{\,r} \end{bmatrix} \quad (37)$$

where ω is the frequency of the fundamental component of the square waves and ω_m is the mechanical speed (equals $\dot{\emptyset}$). Now we define the following:

$$Z_n^{\,s} \triangleq R^s+jn\omega L_\mu{}^s \quad (38)$$

$$Z_n^{\,r} \triangleq R^r+jn\omega L_\mu{}^r \quad (39)$$

$$Z_1 \triangleq Z_n^{\,r} Z_n^{\,s} - (jn\omega L_\mu{}^{sr})^2 \quad (40)$$

$$Z_2 \triangleq \omega_m L_\mu{}^r Z_n^{\,s} - jn\omega_m L_\mu{}^{sr^2} \quad (41)$$

By substituting Equations (38) and (39) in Equation (37) and solving for the currents, the following equations are obtained:

$$\vec{I}_{\alpha_n}^{\,s} = \frac{\vec{V}_{\alpha_n}^{\,s}}{Z_n^{\,s}} \left[1 - \frac{jn\omega L_\mu{}^{sr^2}(n\omega-\omega_m)}{Z_2+jZ_1} \right] \quad (42)$$

$$\vec{I}_{\beta_n}^{\,s} = -j\,\vec{I}_{\alpha_n}^{\,s} \quad (43)$$

$$\vec{I}_{d_n}^{\,r} = \frac{L_\mu{}^{sr}\vec{V}_{\alpha_n}^{\,s}(n\omega-\omega_m)}{Z_2+jZ_1} \quad (44)$$

$$\vec{I}_{q_n}^{\,r} = -j\vec{I}_{d_n}^{\,r} \tag{45}$$

for n = 1, 5, 9, ...

and

$$\vec{I}_{\alpha_n}^{\,s} = \frac{\vec{V}_{\alpha_n}^{\,s}}{Z_n^s}\left[1 + \frac{jn\omega L_\mu^{sr^2}(n\omega+\omega_m)}{Z_2 - jZ_1}\right] \tag{46}$$

$$\vec{I}_{\beta_n}^{\,s} = +j\vec{I}_{\alpha_n}^{\,s} \tag{47}$$

$$\vec{I}_{d_n}^{\,r} = -\frac{L_\mu^{sr}\vec{V}_{\alpha_n}^{\,s}(n\omega+\omega_m)}{Z_2 - jZ_1} \tag{48}$$

$$\vec{I}_{q_n}^{\,r} = j\vec{I}_{d_n}^{\,r} \tag{49}$$

for n = 3, 7, 11, ...

The algebra involved in obtaining Equations (42) through (49) is outlined in Appendix D.

Having these expressions, the contribution of each harmonic to torque may be found. Since only like harmonics interact to produce average torque, it is again possible to consider each harmonic independently and then obtain the total torque by summing the individual contributions.

Consider the n^{th} harmonic. The complex n^{th} harmonic currents in the windings may be represented by a magnitude and a phase angle, for example:

$$\vec{I}_{\alpha_n}^{\,s} \triangleq I_n^s \epsilon^{j\theta^s} \tag{50}$$

If all the currents are written in this form and the instantaneous currents obtained therefrom, the following relations result:

$$i_{\alpha_n}^{s} = I_n^{s} \cos(n\omega t + \theta^{s}) \qquad n = 1,5,9\cdots \tag{51}$$

$$= -I_n^{s} \cos(n\omega t + \theta^{s}) \qquad n = 3,7,11\cdots \tag{51a}$$

$$i_{\beta_n}^{s} = I_n^{s} \cos(n\omega t + \theta^{s} - n\pi/2) = I_n^{s} \sin(n\omega t + \theta^{s}) \qquad n = 1,5,9\cdots \tag{52}$$

$$= -I_n^{s} \cos(n\omega t + \theta^{s} - n\pi/2) = +I_n^{s} \sin(n\omega t + \theta^{s}) \qquad n = 3,7,11\cdots \tag{52a}$$

$$i_{d_n}^{r} = I_n^{r} \cos(n\omega t + \theta^{r}) \qquad n = 1,5,9\cdots \tag{53}$$

$$= -I_n^{r} \cos(n\omega t + \theta^{r}) \qquad n = 3,7,11\cdots \tag{53a}$$

$$i_{q_n}^{r} = I_n^{r} \cos(n\omega t + \theta^{r} - n\pi/2) = I_n^{r} \sin(n\omega t + \theta^{r}) \qquad n = 1,5,9\cdots \tag{54}$$

$$= -I_n^{r} \cos(n\omega t + \theta^{r} - n\pi/2) = I_n^{r} \sin(n\omega t + \theta^{r}) \qquad n = 3,7,11\cdots \tag{54a}$$

Using the above equations and forming the products indicated in Equation (29), we have:

$$i_{\alpha_n}^{s} i_{q_n}^{r} = I_n^{s} I_n^{r} \left[\frac{\sin(\theta^{r} - \theta^{s})}{2} + \frac{\sin(2n\omega t + \theta^{s} + \theta^{r})}{2}\right] \qquad n = 1,5,9\cdots \tag{55}$$

$$= -I_n^{s} I_n^{r} \left[\frac{\sin(\theta^{r} - \theta^{s})}{2} + \frac{\sin(2n\omega t + \theta^{s} + \theta^{r})}{2}\right] \qquad n = 3,7,11\cdots \tag{55a}$$

$$i_{\beta_n}^{s} i_{d_n}^{r} = I_n^{s} I_n^{r} \left[\frac{\sin(\theta^{s} - \theta^{r})}{2} + \frac{\sin(2n\omega t + \theta^{s} + \theta^{r})}{2}\right] \qquad n = 1,5,9\cdots \tag{56}$$

$$= -I_n^{s} I_n^{r} \left[\frac{\sin(\theta^{s} - \theta^{r})}{2} + \frac{\sin(2n\omega t + \theta^{s} + \theta^{r})}{2}\right] \qquad n = 3,7,11\cdots \tag{56a}$$

The time-varying terms in the above equations produce no average torque. Substituting average values in Equation (29), the following expressions for average electromechanical torque result:

$$T_{e_n} = \frac{P}{2} L_\mu^{sr} \left[I_n^s I_n^r \sin(\theta^s - \theta^r) \right] \qquad n = 1,5,9\cdots \qquad (57)$$

$$= \frac{P}{2} L_\mu^{sr} \left[-I_n^s I_n^r \sin(\theta^s - \theta^r) \right] \qquad n = 3,7,11\cdots \qquad (57a)$$

This result is not particularly useful, but it can be converted to useful form if we consider the following:

$$\vec{I}_{\alpha_n}^{\,s} \vec{I}_{q_n}^{\,r*} = I_n^s \epsilon^{j\theta^s} I_n^r \epsilon^{-j(\theta^r - n\pi/2)} = I_n^s I_n^r \left[-\sin(\theta^s - \theta^r) + j\cos(\theta^s - \theta^r) \right] \quad n = 1,5,9\cdots (58)$$

$$= -I_n^s \epsilon^{j\theta^s} \left[-I_n^r \epsilon^{-j(\theta^r - n\pi/2)} \right] = -I_n^s I_n^r \left[-\sin(\theta^s - \theta^r) + j\cos(\theta^s - \theta^r) \right] \quad n = 3,7,11\cdots (58a)$$

Similarly:

$$\vec{I}_{\beta_n}^{\,s*} \vec{I}_{d_n}^{\,r} = I_n^s \epsilon^{-j(\theta^s - n\pi/2)} I_n^r \epsilon^{j\theta^r} = I_n^s I_n^r \left[\sin(\theta^s - \theta^r) + j\cos(\theta^s - \theta^r) \right] \quad n = 1,5,9\cdots (59)$$

$$= -I_n^s \epsilon^{-j(\theta^s - n\pi/2)} \left[-I_n^r \epsilon^{j\theta^r} \right] = -I_n^s I_n^r \left[\sin(\theta^s - \theta^r) + j\cos(\theta^s - \theta^r) \right] \quad n = 3,7,11\cdots (59a)$$

So we can write:

$$-\vec{I}_{\alpha_n}^{\,s} \vec{I}_{q_n}^{\,r*} + \vec{I}_{\beta_n}^{\,s*} \vec{I}_{d_n}^{\,r} = 2 I_n^s I_n^r \sin(\theta^s - \theta^r) \qquad n = 1,5,9\cdots \qquad (60)$$

$$= -2 I_n^s I_n^r \sin(\theta^s - \theta^r) \qquad n = 3,7,11\cdots \qquad (60a)$$

The right hand side of the above equations is of the same form as the bracketed terms in Equations (57) and (57a).

Using Equations (43), (45), (47), and (49), we now write:

$$-\vec{I}_{\alpha_n}^{s}\vec{I}_{q_n}^{r*}+\vec{I}_{\beta_n}^{s*}\vec{I}_{d_n}^{r}=-\vec{I}_{\alpha_n}^{s}\vec{I}_{q_n}^{r*}-\vec{I}_{\alpha_n}^{s*}\vec{I}_{q_n}^{r}=2\,\mathcal{R}e\left[-\vec{I}_{d_n}^{s}\vec{I}_{q_n}^{r*}\right]\qquad n=1,3,5\cdots \tag{61}$$

Combining the developments of Equations (57) through (61), we obtain the following expression for torque.

$$Te_n=\frac{P}{2}L_\mu^{sr}\,\mathcal{R}e\left[-\vec{I}_{\alpha_n}^{s}\vec{I}_{q_n}^{r*}\right]\qquad n=1,3,5,\cdots \tag{62}$$

Performing the operations required by the above equation, we find:

$$Te_n=\frac{P}{2n\omega s_n}\left\{\frac{\vec{V}_{\alpha_n}^{s2}L_\mu^{sr2}R^r}{\left[\frac{L_\mu^{s}R^r}{s_n}+L_\mu^{r}R^s\right]^2+\left[\frac{R^rR^s}{n\omega s_n}+n\omega\left(L_\mu^{sr2}-L_\mu^{r}L_\mu^{s}\right)\right]^2}\right\} \tag{63}$$

$n=1,5,9\cdots$

where
$$s_n\triangleq\frac{n\omega-\omega_m}{n\omega} \tag{64}$$

$$Te_n=\frac{P}{2n\omega s_n'}\left\{\frac{\vec{V}_{\alpha_n}^{s2}L_\mu^{sr2}R^r}{\left[\frac{L_\mu^{s}R^r}{s_n'}+L_\mu^{r}R^s\right]^2+\left[\frac{R^rR^s}{n\omega s_n'}+n\omega\left(L_\mu^{sr2}-L_\mu^{r}L_\mu^{s}\right)\right]^2}\right\} \tag{65}$$

$n=3,7,11\cdots$

where
$$s_n'\triangleq\frac{n\omega+\omega_m}{n\omega} \tag{66}$$

Again, the algebra involved in obtaining these equations is outlined in Appendix D.

Now, the results given in Equations (63) and (65) must be interpreted. There is no difficulty in interpreting Equation (63); harmonics 1, 5, 9, etc., all give rise to normal motor action, operating with a slip less than one. With regard to Equation (65), it is seen that motor action is produced by harmonics 3, 7, 11, etc., also, but in a direction opposite to the direction of rotation.

This result could have been predicted from consideration of the direction of rotation of the various harmonic fluxes. In Fig. XIII are shown the fundamental and two harmonics of

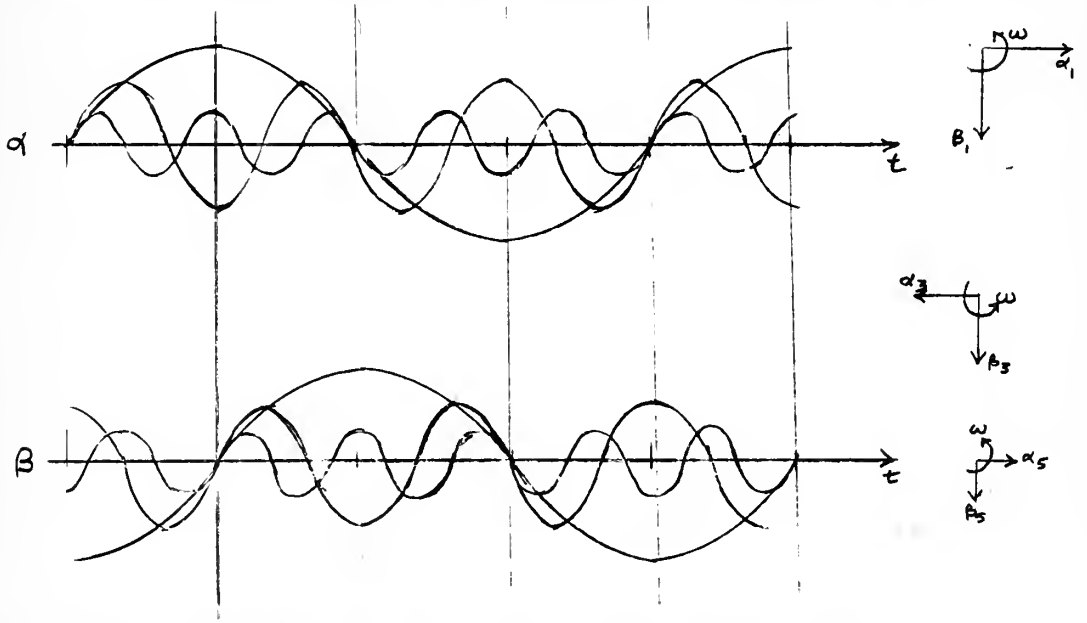

Fig. XIII. Fundamental and first two harmonics of two square waves displaced 90° in time.

two square waves displaced 90° in time. If the α wave is taken as the reference, vectors for the various components may be drawn, as shown in Fig. XIII, for t = 0. We see that in the first, fifth, etc., harmonic, the α wave leads the β wave, whereas the α wave lags the β wave in the third,

seventh, etc., harmonics. The effect of the latter is to produce waves traveling in the reverse direction. Therefore, the resultant flux travels in the reverse direction with the result that negative torque is produced. In effect, the negative torque-producing harmonics have reversed the leads to the motor.

It must be determined whether this negative torque is of sufficient importance to necessitate consideration of introducing filters into the circuit to remove the harmonic content of the switching circuit output. Substituting the expressions for the exciting voltage from Equation (32) in the torque expressions, we find:

$$Te_n = \frac{P}{2}\left(\frac{16V^2}{\pi^2}\right)\frac{1}{n^3\omega s_n}\left\{\frac{L_\mu^{sr^2}R^r}{\left[\frac{L_\mu^s R^r}{s_n}+L_\mu^r R^s\right]^2+\left[\frac{R^r R^s}{n\omega s_n}+n\omega\left(L_\mu^{sr^2}-L_\mu^r L_\mu^s\right)\right]^2}\right\}_{n=1,5,9\cdots} \tag{67}$$

$$=-\frac{P}{2}\left(\frac{16V^2}{\pi^2}\right)\frac{1}{n^3\omega s_n'}\left\{\frac{L_\mu^{sr^2}R^r}{\left[\frac{L_\mu^s R^r}{s_n'}+L_\mu^r R^s\right]^2+\left[\frac{R^r R^s}{n\omega s_n'}+n\omega\left(L_\mu^{sr^2}-L_\mu^r L_\mu^s\right)\right]^2}\right\}_{n=3,7,11\cdots} \tag{67a}$$

The appearance of the factor, n^3, in the denominator indicates that the harmonics may not be too important as regards torque production. It is not possible to make any absolute statement in this regard, however, for the importance of the various harmonics will depend on the relative magnitudes of the parameters of any given machine.

In order to illustrate the effects of the harmonics, however, the torque-speed curve for motor action in the frequency range of the fundamental was calculated for arbitrarily assumed values of the various parameters. In order to get a picture of the curves over the entire speed range, maximum torque produced by each harmonic was also calculated. These calculations, given in Appendix D, result in torque-speed curves of the form shown in Fig. XIV.

For this particular assumed machine, we see that the harmonics have negligible effect torque-wise on operation. This result cannot be applied to the general case; rather, curves such as those shown in Fig. XIV should be calculated for any given machine of interest in order to determine the importance of the various harmonics in torque production.

Now, the above analysis is for the case of a two-phase machine with balanced two-phase excitation. Early in this chapter it was stated that this result could be used to obtain the expressions for the three-phase machine by making a symmetrical component transformation. This is true, but the process would be long and tedious. We can apply the two-phase result qualitatively to the three-phase case by realizing that the primary effect of going to three-phase machine is to change the phase relationships of the various harmonics. Again consider the rotating fields which are set up in this case. In Fig. XV are shown the fundamental and two harmonics of three square waves displaced 120° in time. We observe that the first,

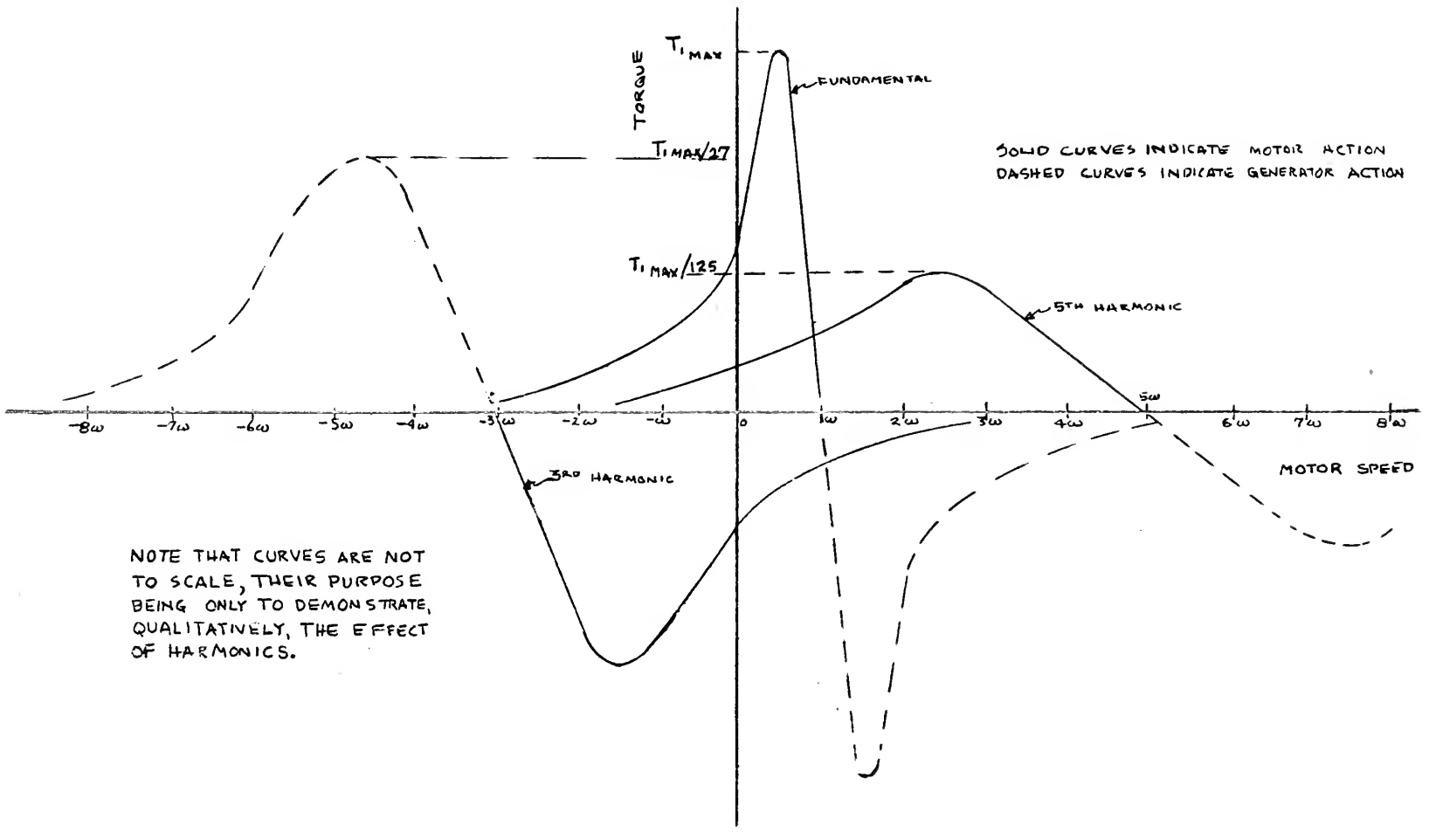

Fig. XIV. Torque-speed curves for fundamental and first two harmonics of torque produced by square wave excitation.

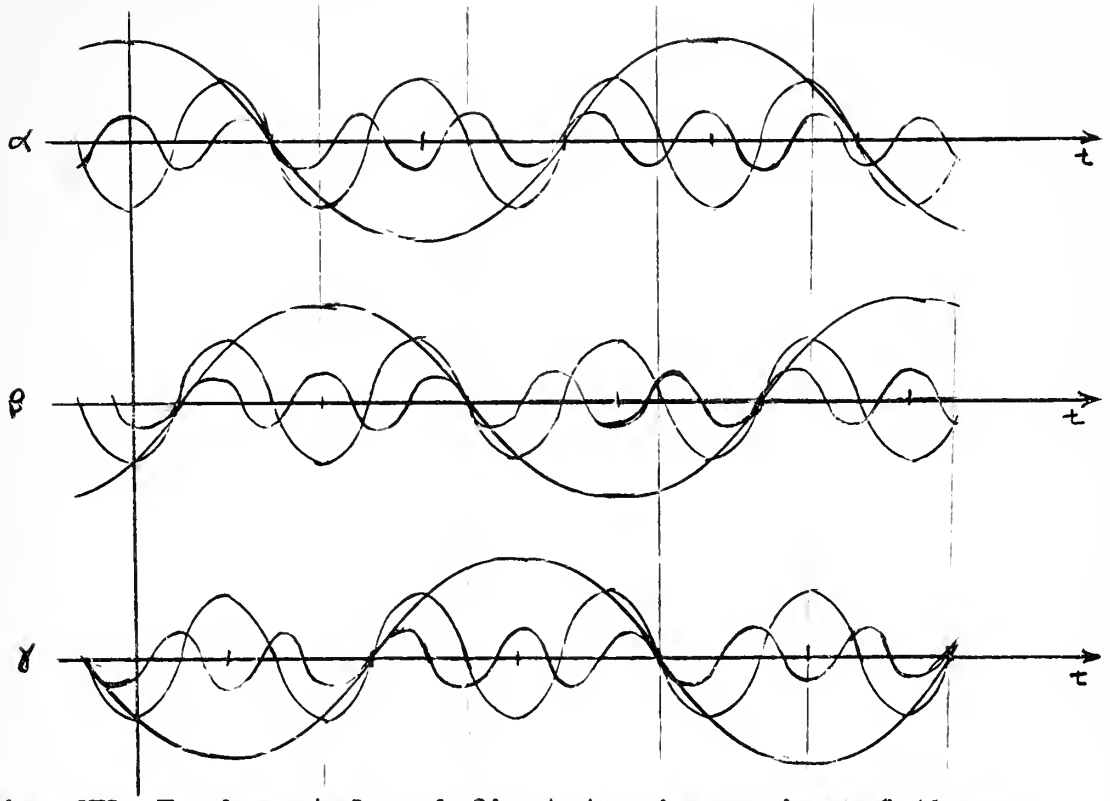

Fig. XV. Fundamental and first two harmonics of three square waves displaced 120° in time.

seventh, thirteenth, etc., harmonics produce motor action in the direction of rotation, whereas the fifth, eleventh, seventeenth, etc., produce motor action opposing rotation. The third, ninth, etc., harmonics are in phase, hence produce no torque.

So in the case of the three-phase machine excited by balanced three-phase square wave voltages, the harmonics have negligible effect in producing torque, since each harmonic torque will be attenuated roughly as the reciprocal of the third power of the order number of the harmonic. Since these harmonics contribute little to torque production, it may be best to filter them out of the square wave and apply

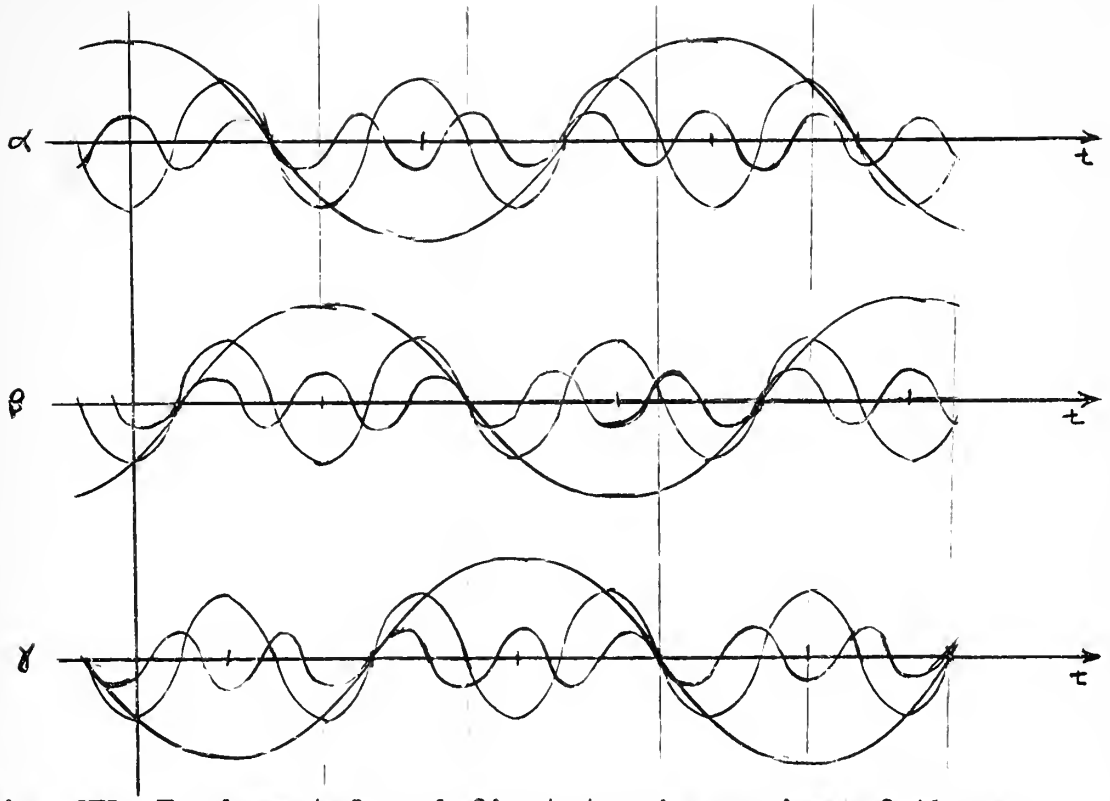

Fig. XV. Fundamental and first two harmonics of three square waves displaced 120° in time.

seventh, thirteenth, etc., harmonics produce motor action in the direction of rotation, whereas the fifth, eleventh, seventeenth, etc., produce motor action opposing rotation. The third, ninth, etc., harmonics are in phase, hence produce no torque.

So in the case of the three-phase machine excited by balanced three-phase square wave voltages, the harmonics have negligible effect in producing torque, since each harmonic torque will be attenuated roughly as the reciprocal of the third power of the order number of the harmonic. Since these harmonics contribute little to torque production, it may be best to filter them out of the square wave and apply

only the fundamental to the induction motor. Whether or not this is important will be shown in the next section, where losses are discussed.

6.4 Losses Due to Harmonic Content of Applied Voltage

The rotor copper loss due to any n^{th} harmonic may be represented by the following relation [6]:

$$P_{Loss} = S_n n\omega Te_n \tag{68}$$

Using Equations (67) and (67a), this can be written as:

$$P_{Loss} = \frac{P}{2}\left(\frac{16V^2}{\pi^2}\right)\frac{1}{n^2}\left\{\frac{L_\mu{}^{sr^2} R^r}{\left[\frac{L_\mu{}^s R^r}{S_n} + L_\mu{}^r R^s\right]^2 + \left[\frac{R^r R^s}{n\omega S_n} + n\omega\left(L_\mu{}^{sr^2} - L_\mu{}^r L_\mu{}^s\right)\right]^2}\right\} \tag{69}$$

As in the case of harmonic contributions to torque, the importance of this loss depends upon the parameters of the particular machine being considered. In order to get some idea of the importance of the losses, calculations are made in Appendix D for the machine already considered. In the calculation, it is assumed that the motor is operating at a slip of 10% relative to the fundamental.

The calculation shows that, considering only the fundamental and first two harmonics, efficiency (neglecting other losses) falls from 90% with the fundamental alone to 72.5% when the fundamental and first two harmonics are included. Presumably the effect is even more pronounced when more harmonics are considered. Furthermore, the harmonics develop relatively large rotor copper losses,

contributing, in fact, far more power to undesirable heating than to mechanical power to the load.

We can conclude, therefore, that, although the harmonic content in the voltage has negligible effect on torque-speed characteristics, the power losses associated with these harmonics are of appreciable magnitude, possibly larger than those contributed by the fundamental. Therefore, it is desirable to filter the harmonics out of the switching-circuit output and apply only the fundamental to the induction motor.

6.5 Effect of Varying Line Frequency and Voltage on Maximum Torque

In this section only the fundamental component of applied voltage will be studied. The harmonics have little effect on torque and, as was shown in the preceding section, are actually undesirable from the standpoint of efficiency and heating and should be filtered out.

From Equation (67), the expression for the torque produced by the fundamental is:

$$T_e = \frac{P}{2}\left(\frac{16V^2}{\pi^2}\right)\frac{1}{\omega s}\left\{\frac{L_\mu^{sr2}R^r}{\left[\frac{L_\mu^s R^r}{s}+L_\mu^r R^s\right]^2+\left[\frac{R^r R^s}{\omega s}+\omega\left(L_\mu^{sr2}-L_\mu^r L_\mu^s\right)\right]^2}\right\} \quad (70)$$

It is desired to determine the effect of varying frequency and magnitude of applied voltage on the maximum torque produced. In Appendix D it is shown that the slip for maximum torque is:

$$S_m = \pm R^r\sqrt{\frac{(\omega L_\mu^s)^2+R^{s2}}{(\omega L_\mu^r R^s)^2+\omega^4(L_\mu^r L_\mu^s-L_\mu^{sr2})^2}} \quad (71)$$

Equation (70) may be rewritten as follows:

$$Te = \frac{P}{2}\left(\frac{16V^2}{\pi^2}\right)\frac{L_\mu^{sr^2}R^r}{\omega}\left[\frac{S}{(R^rL_\mu^s)^2+\left(\frac{R^rR^s}{\omega}\right)^2+S(2R^rR^sL_\mu^{sr^2})+S^2\left[(L_\mu^rR^s)^2+\omega^2(L_\mu^{sr^2}-L_\mu^rL_\mu^s)^2\right]}\right] \quad (72)$$

Substituting (71) and (72) and solving, we obtain:

$$Te_m = \frac{P}{4}\left(\frac{16V^2}{\pi^2}\right)\frac{L_\mu^{sr^2}}{\omega R^sL_\mu^{sr^2}+\sqrt{\left[(\omega L_\mu^s)^2+R^{s^2}\right]\left[\omega^2(L_\mu^rL_\mu^s-L_\mu^{sr^2})^2+(L_\mu^rR^s)^2\right]}} \quad (73)$$

For the particular machine studied in Appendix D, the above equation shows that the maximum torque increases in direct proportion to the increase in frequency (since when frequency is doubled, input voltage is doubled, etc.), but this is because the inductances were assumed to be equal. In most practical cases, however, the inductance difference term in Equation (73) would be of considerable magnitude with the result that the maximum torque would remain very nearly constant as voltage and frequency are varied simultaneously and in the same direction.

6.6 Conclusions Concerning Square Wave Excitation of Induction Machine

Based upon the foregoing, the following general conclusions are made:

1. Time harmonics in square-wave voltage excitation of an induction machine have no appreciable effect on the torque-speed characteristics in the speed range of the fundamental component of voltage.

2. For both two-phase and three-phase machines, the cumulative effect of all the harmonics is to decrease slightly the torque available at any given speed, since the harmonics which produce the largest torque oppose the motion of the machine.

3. The rotor copper loss due to harmonics is appreciable, being of such magnitude as to decrease efficiency somewhat and to produce considerable heating.

Summing up the conclusions, we can say that the overall effect of harmonics is bad. If possible, they should be filtered out of the switching-circuit output, leaving only the fundamental to be applied to the induction motor.

CHAPTER 7

EXPERIMENTAL RESULTS

7.1 Outline of Procedure

The experimental phase of this thesis may be separated into four divisions:

1. Design of the circuit.
2. Investigation of parameter changes necessary to obtain good oscillation and wave form for a single converter.
3. Investigation of the effects of parameter changes with a three-phase circuit.
4. Operation of an induction motor.

7.2 Design of Circuit and Procedure for Test

The original circuit was designed primarily on the basis of papers by Royer [1] and Milnes [2]. No attempt was made to optimize the design, liberal safety factors being included to ensure operation. Due to restricted time available for winding and assembly of cores, the circuit design was not refined after initial design, except that the resistance introduced into the base in the phase-locking circuit was varied to obtain best results. Details of the design are outlined in Appendix E.

It has been noted in the preceding chapters of this thesis that the interacting influences of control voltage (E), load resistance (R_L), base resistance ($R+R_b$), and the number of phases have a definite influence on the ability of the

converters to oscillate and on the frequency of oscillations. In investigating these interactions a single phase converter was built first and tested. Then two converters were phase-locked 120° out of phase, and finally three converters were phase-locked to form the desired three-phase square wave output. The results of these investigations are shown below in graphical form. An explanation of the results is included which refers to the theory developed in preceding chapters.

7.3 Single Phase Converter

The circuit used was that shown in Fig. I, Chapter 3. Fig. XVI below shows that the output frequency of a converter is directly proportional to the control voltage, other parameters being constant. This figure also shows that the amount of resistance in the base has a large effect on the value of the output frequency. Since the base resistance was fixed by the selection of transistor and core windings, variation in R_b was simulated by adding extra resistance to the base circuit. This effect is predicted analytically by Equation (11), Chapter 3. As the total base resistance becomes much larger than R_s, the value of V_1 approaches E, the applied voltage, so that the output frequency approaches more nearly the ideal predicted frequency.

Fig. XVII indicates that the value of load impedance also effects the value of the output frequency. By increasing the load the frequency more nearly approaches the value given by the simple Equation (21). Reference to Fig. V

shows that as the load is varied, the voltage, V_1, which is impressed on the core changes slightly, thus changing the output frequency. This effect is not nearly as significant as the effect of reflected base resistance and can be considered negligible.

Each of the three converters to be used in the three-phase circuit was tested separately. As far as could be determined each converter exhibited identical frequency characteristics as variations in parameters were made.

7.4 The Two-phase Circuit

The schematic diagram for the two-phase circuit is shown in Fig. VIII, Chapter 4. The same variation of parameters was made for circuit as is described in Section 7.2. However, the slope of the frequency versus control voltage curve was somewhat greater than for the single phase case. It was also noted that the range of operation was somewhat less than in the three-phase case. The results are shown in Figs XVIII and XIX. The interpretation of these results will be dealt with more fully in the discussion of three-phase operation.

7.5 The Three-phase Circuit

The schematic diagram for the three-phase circuit is shown in Fig. X, Chapter 5. The results of tests for this circuit are shown in Figs XVIII, XIX, XX, XXI, and XXII.

7.51 Effect of Load Resistance (R_L) on Frequency

In discussing single-phase operation it was shown that the load resistance had a definite effect on output

frequency. As can be seen from Fig. XVIII, increasing the phases lessens the effect. That is, by increasing the phases the frequency of the output more nearly agrees with the values given by the simple Equation (21). Although this was not investigated analytically, and it would seem to be extremely difficult to follow the effect of reflected load impedances in the circuit, the explanation appears to be the same as that given in Section 7.2. However, this variation is a minor one being only 2 percent for a change in load by a factor of 10.

7.52 Effect of Added Base Resistance (R) on Frequency

In discussing the single phase circuit it was shown that the effect of added base resistance was to make the output frequency more nearly approach the values given by the Equation (21). The effect for the three-phase case is more pronounced because R_b itself is increased by reflected impedances from the many more resistances in the circuit. This effect can be seen from Fig. XXI, where in changing this resistance by a factor of 11 to 1 (from 5 to 55 ohms) only causes a variation in frequency of 2.6%. Thus it can be inferred that when designing a converter for three-phase operation, the design can be based on Equation (21) without being too much in error. It was also noted that the frequency is directly proportional to the control voltage, in so far as the measurement techniques used in the testing could detect.

7.53 Effect of Circuit Parameters on Range of Oscillation

It has been pointed out in earlier chapters that the circuit will not oscillate unless the parameters are such that the reciprocal of the load resistance ($1/R_L$) is less than the slope of the negative resistance portion of the converter characteristics. The negative resistance (R_o') is a function of the number of phases, the total base resistance (R_b+R), the load resistance (R_L) and the control voltage. Using Equation (19), together with the definition of K in Equation (20), it can be seen that with fixed parameter values, the negative resistance will vary with the control voltage E. This means first that there is a minimum load resistance for oscillation, assuming the upper limit on E is set by the transistor, and secondly, that when the load resistance is such that oscillation occurs at maximum voltage there will be a point at which oscillation will cease as the control voltage decreases. This is verified experimentally as shown in Fig. XXII. Referring to the figure, the area marked "Range of No Oscillation" includes the combinations of R and R_L for which oscillation will not occur at the maximum control voltage (20 volts for the circuit described). The curves to the left of this region show the possible combinations of R_L and R_b for which oscillation will occur for values of control voltage from maximum down to the value listed as parameters on each curve.

It should be pointed out that actually determining the range of oscillation was complicated by the fact that voltages tended to go out of phase at low values of control voltage. No theoretical explanation of this effect is known, it being assumed that non-linear effects come into the picture at low voltages.

7.54 Effect of Number of Phases on Frequency

As mentioned before no analysis of the effect of phases on frequency was made because of the complexity of the problem. However, it is an experimental fact that adding phases lessens the effect on the output frequency of the other main parameters (R_L and R).

7.55 Effect of Inductive Load

Several runs were made with inductive load consisting of a series combination of resistance and inductance. However, the effect on output frequency was minor and the overall effect did not appear to be dependent on type of inductive load. The power factors of the loads varied from 1.0 down to approximately 0.85.

7.6 Operation of an Induction Motor with Circuit Output

One of the objectives of the thesis was to determine the feasibility of operating an induction motor with output of this three-phase switching circuit. Since the power level of the output of the circuit was limited to a maximum of 40 watts per phase by the transistor characteristics, it was not possible to obtain a polyphase induction machine of small enough size to use with the circuit. Nevertheless it

was possible to simulate an induction machine with a synchro control transformer by shorting the rotor leads. This was done with a synchro transformer whose nameplate data was:

SYNCHRO CONTROL TRANSFORMER, 1CT MK5, Mod. 4
USN BuOrd Dwg. 292874, Ser. No. 9419 90/55
Volts a.c. 60 cps. Bendix Aviation Corp.

Since the square wave output has a voltage magnitude of about 20 volts, it was decided to connect the three-phase of the circuit in a Y-connection to approach as closely as possible the value of 55 volts listed on the nameplate.

The input impedance of the motor was measured at approximately 15 ohms. Several attempts were made to run the motor with an added base resistance (R) of 50 ohms without success. When the added base resistance was reduced to 5 ohms operation was possible. The results are shown in Fig. XXII. Operation was only possible for a range of control voltage from 15 to 20 volts. At the lower range of voltages the operation became erratic and the motor usually stopped suddenly indicating a lack of sufficient torque.

7.7 General Comments

It is felt that it should be pointed out that the circuit for three-phase operation is rather complicated and presents some difficulty to those who desire to set it up. Further, it was found that the circuit sometimes would present variations in behavior from day to day. One peculiarity is that at times the circuit would jump out of phase when control voltage was reduced to low values. When

voltage was increased the phase locking did not reappear. It was found that by disconnecting any two leads in the phase-locking circuit and grounding them, phase-locking action occurred once more when the circuit was re-energized. A variable condenser was used at several places in the circuit in an attempt to correct this because it was felt that a charge was being built up in the phase locking circuit. A .05 microfarad condenser across the emitter to collector terminals somewhat alleviated this situation. However, the best results were usually gotten when tests were resumed on a different day.

Another difficulty experienced was with faulty operation of the transistors. It appeared that one of the transistors failed progressively. The first effect noted was a reduction in circuit output frequency from previous values. Aside from this effect the circuit appeared to be operating normally. Later in the test program it was found that it wasn't possible to get full control voltage across the circuit. It was apparent that something was presenting a short in the circuit when control voltage reached 18-20 volts. It was found to be caused by one of the transistors, replacement of which restored the circuit to normal operation.

Thus, we can conclude that even with an understanding of the circuit based on fairly rigorous analysis, experimental results are difficult to obtain simply because the circuit, being an intricate complex of non-linear elements, often behaves in an unpredictable manner. While the circuit holds promise, much more experimental work is required.

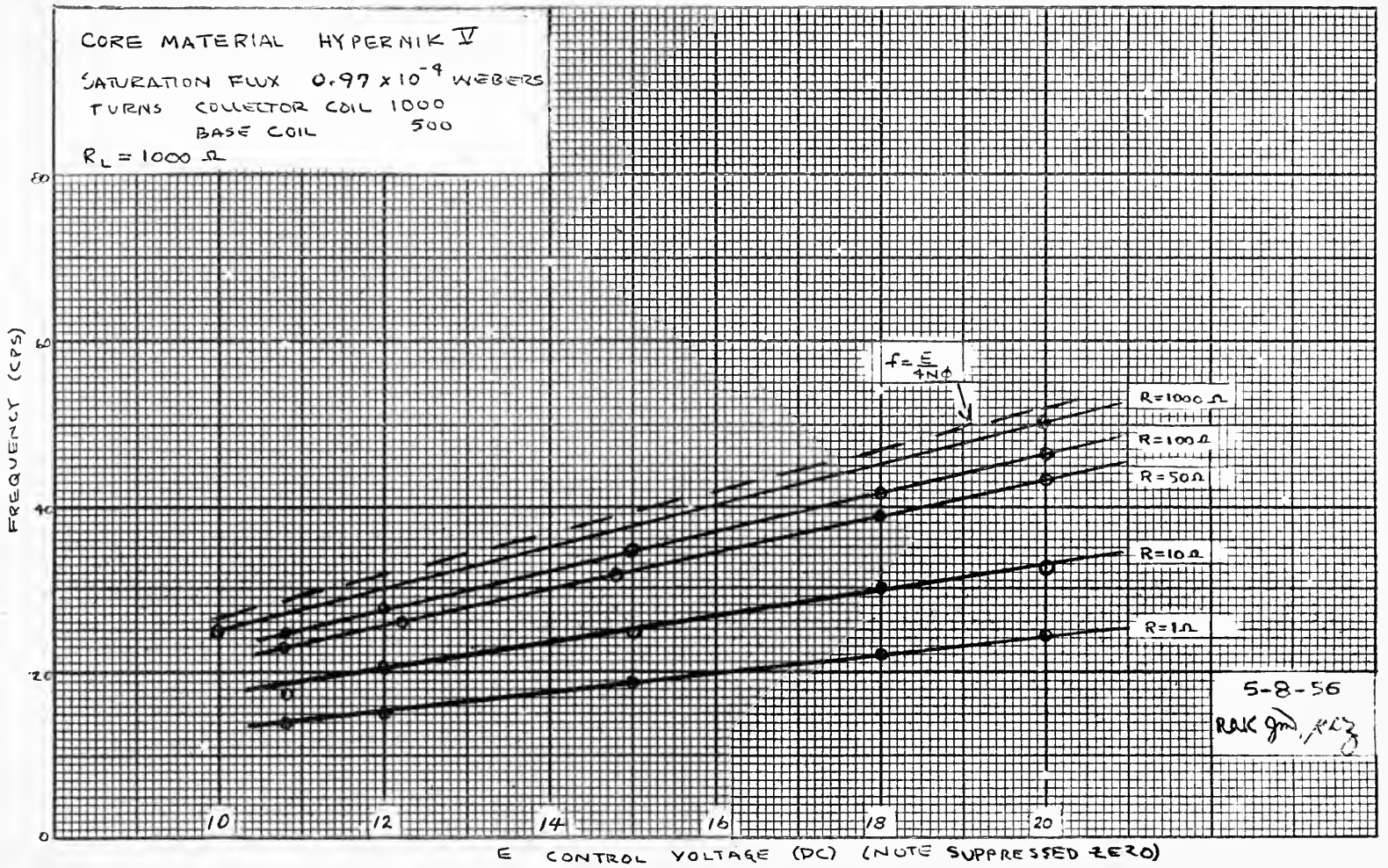

Fig. XVI. Effect of adding base resistance on output frequency of single converter.

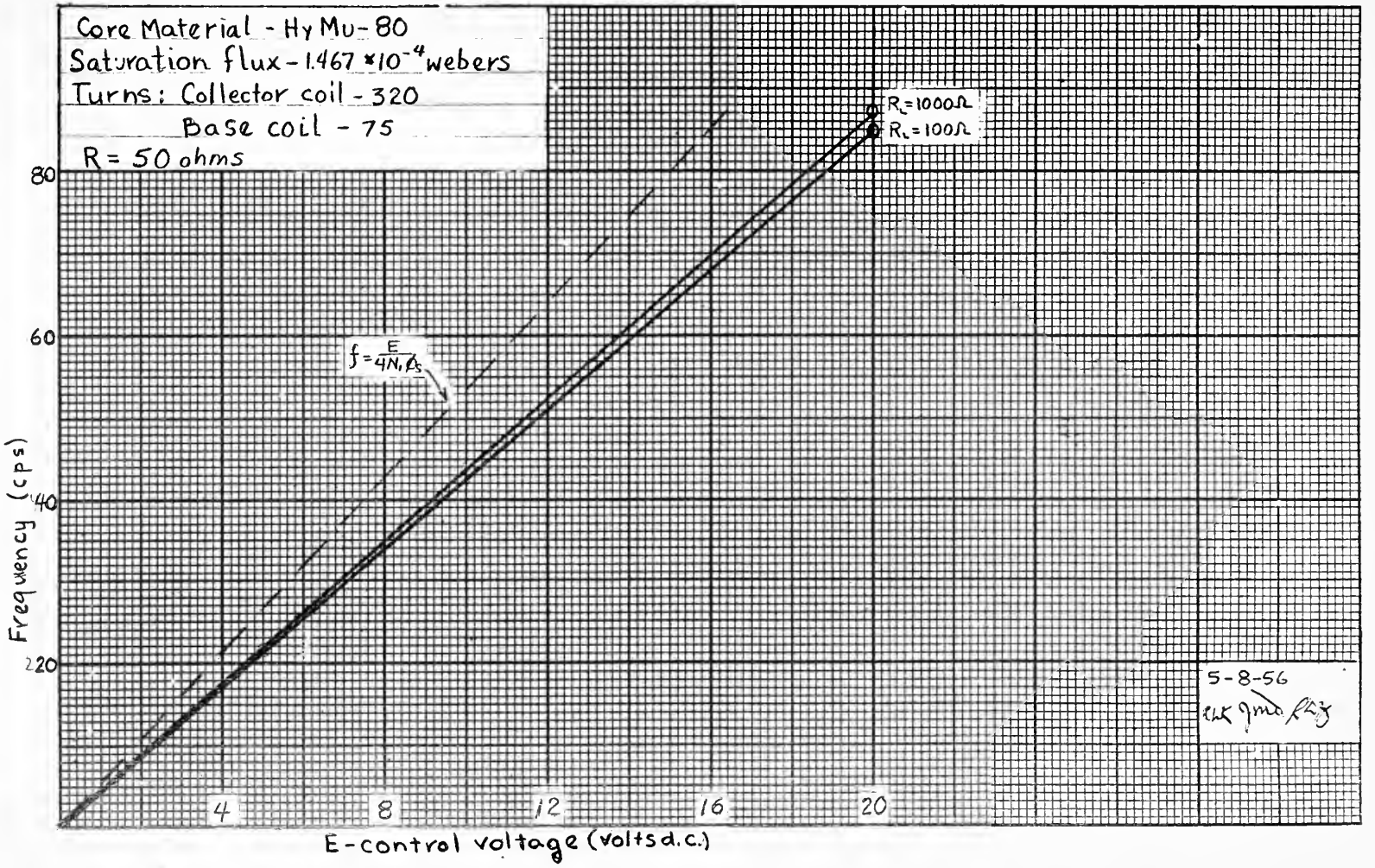

Fig. XVII. Effect of load resistance (R_L) on output for three-phase circuit.

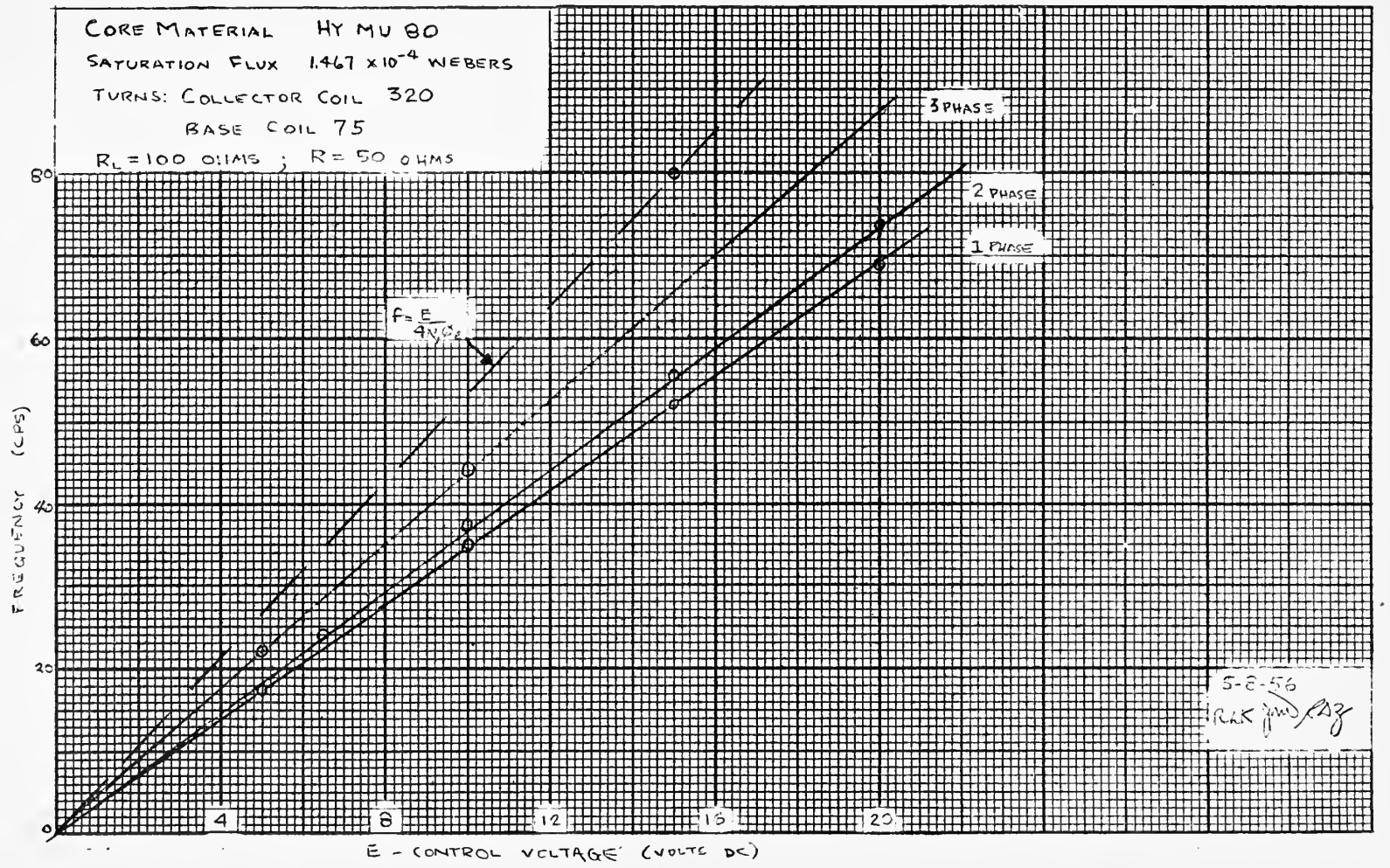

Fig. XVIII. Effect of number of phases in circuit on output frequency.

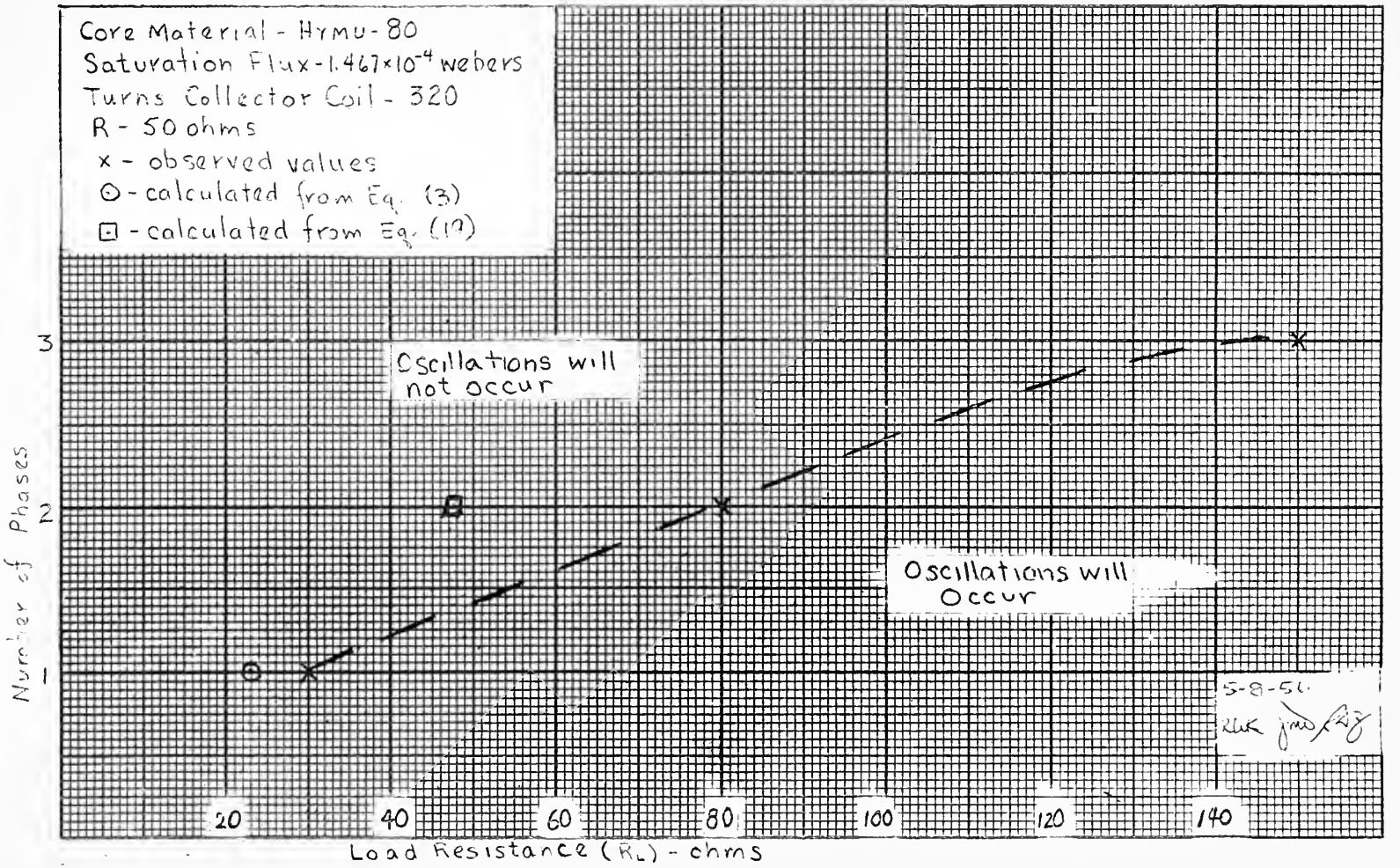

Fig. XIX. Effect of load and number of phases on probability of oscillation.

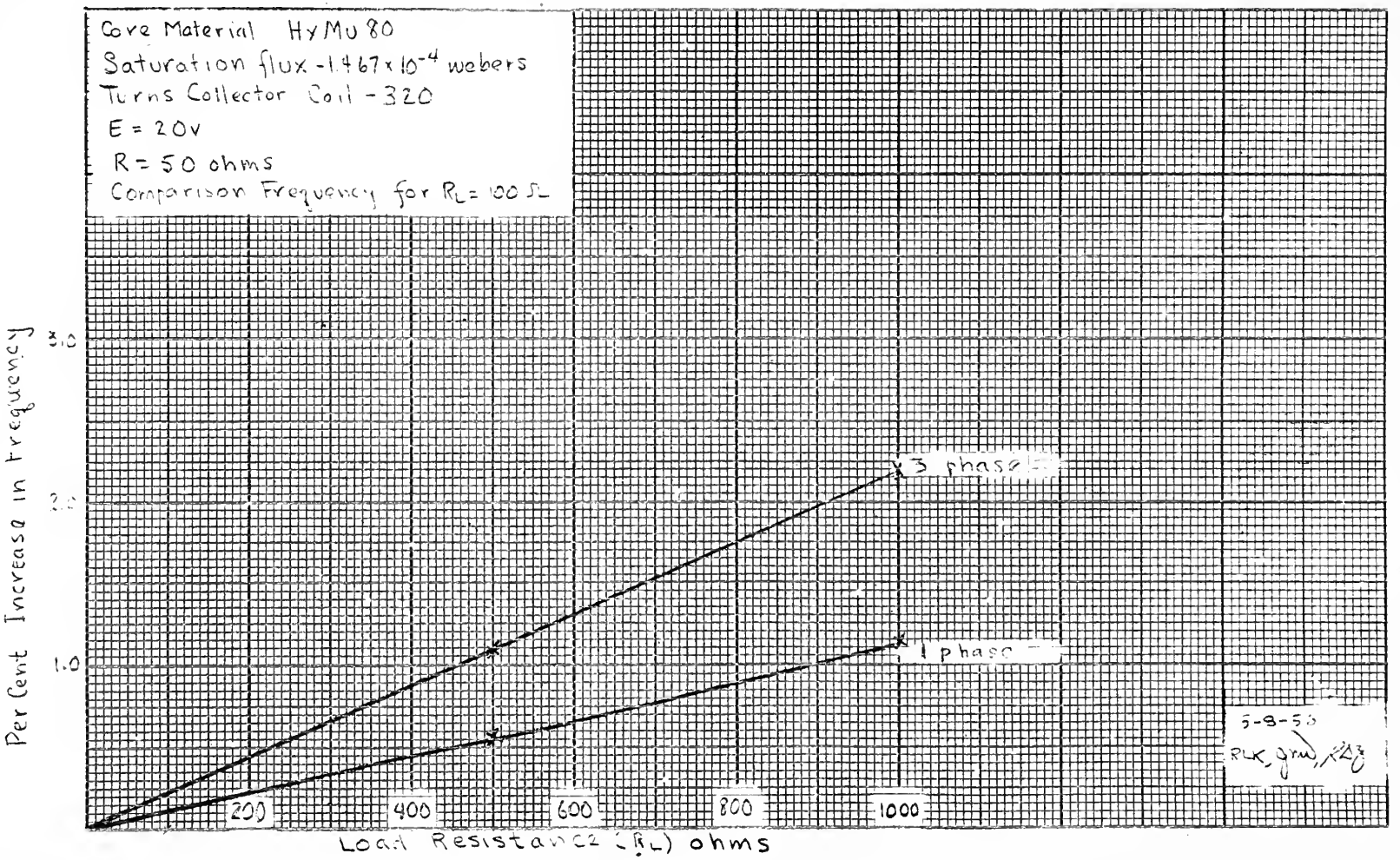

Fig. XX. Effect of load resistance, R_L, on frequency.

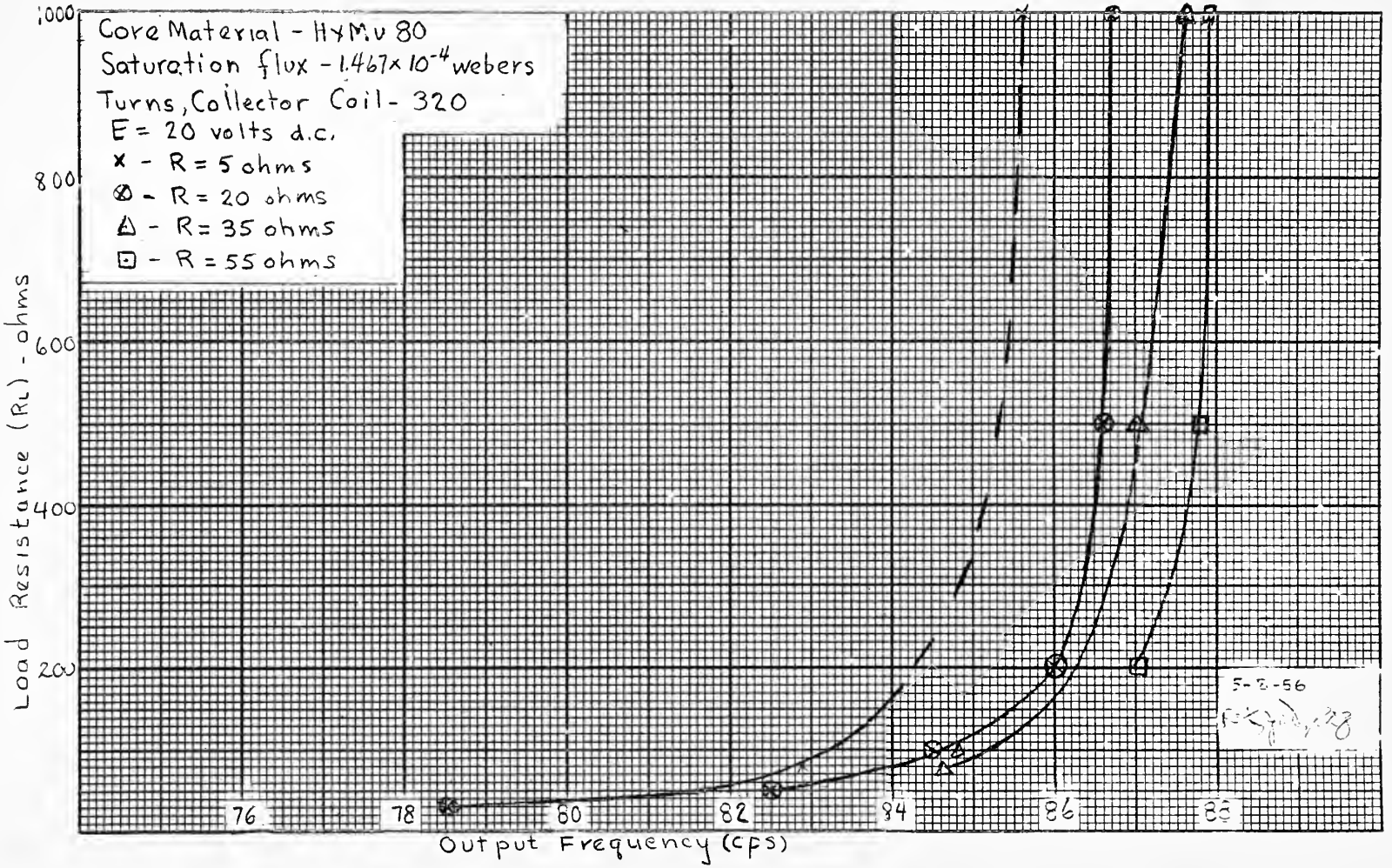

Fig. XXI. Effect of load resistance on maximum frequency of three phase circuit.

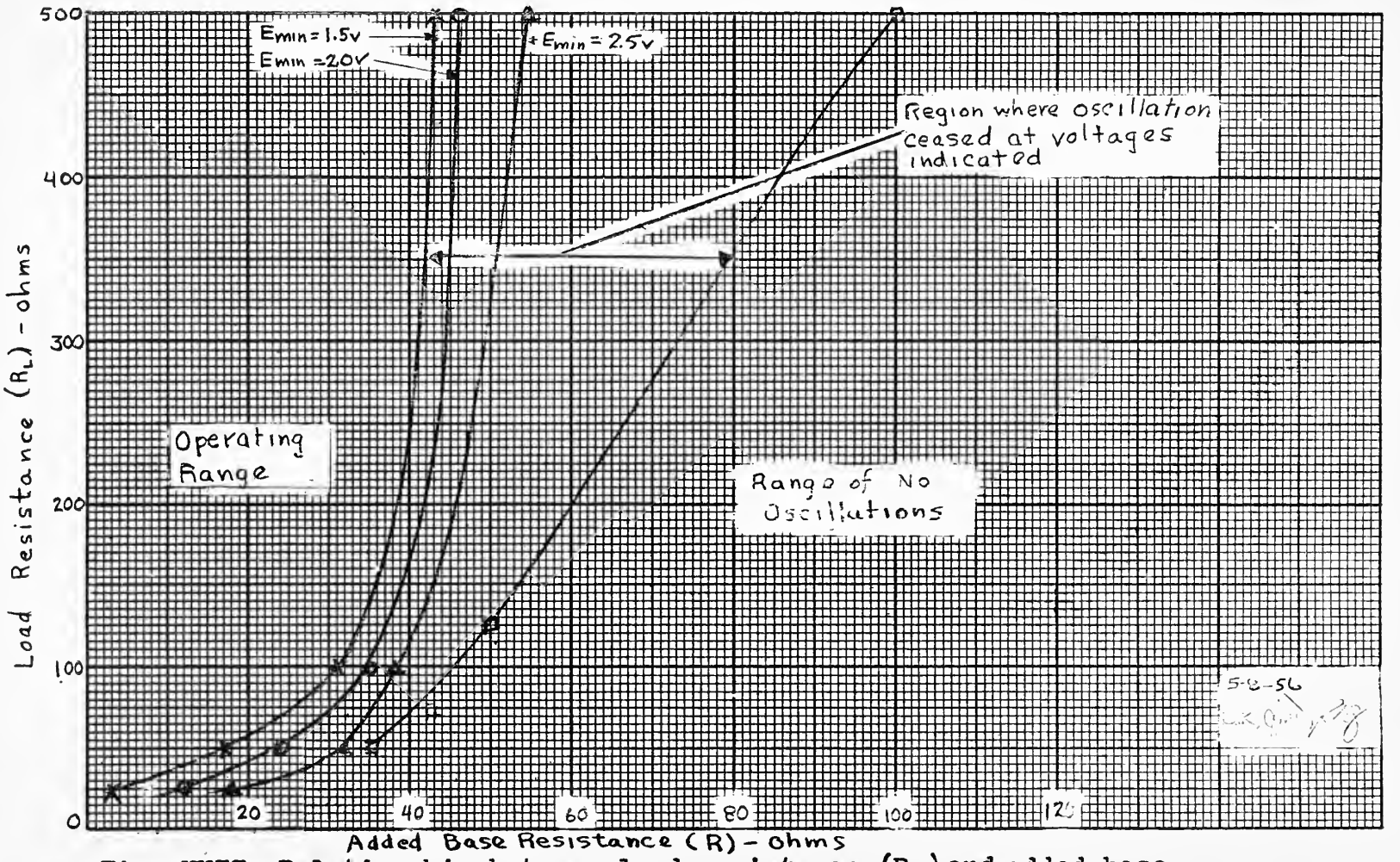

Fig. XXII. Relationship between load resistance (R_L) and added base resistance (R) needed to insure oscillation.

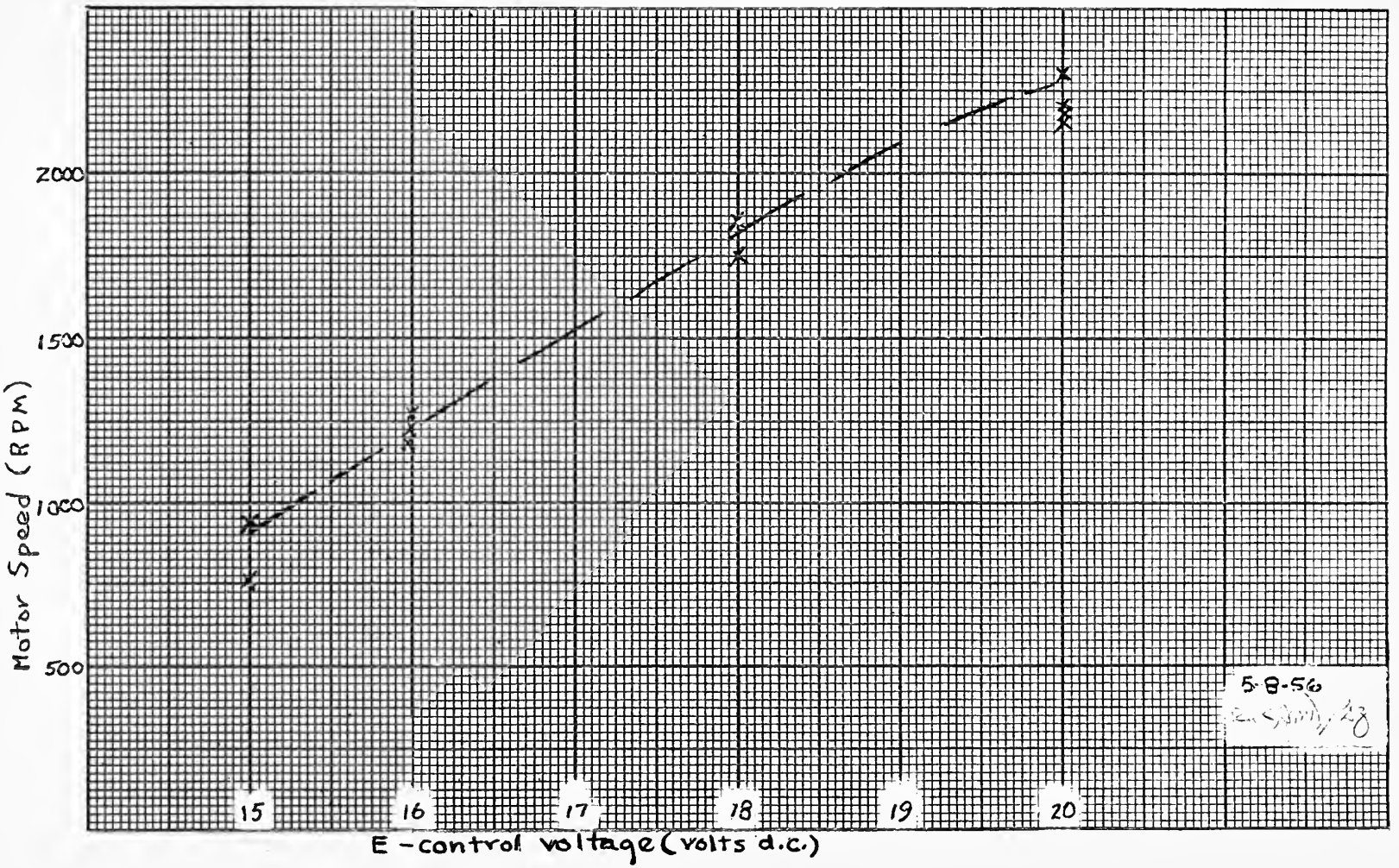

Fig. XXIII. Speed of an induction motor versus control voltage.

CHAPTER 8

CONCLUSIONS AND RECOMMENDATIONS

8.1 Conclusions

The following conclusions are made with regard to the study pursued in this thesis:

1. For any given circuit parameters and number of phases, the switching-circuit range of operation is load dependent. The effect of numbers of phases is shown clearly in Fig. XIX wherein it is shown that oscillations will occur with a load resistance of thirty ohms for the single-phase case, whereas a load of 150 ohms is required to obtain oscillatory action in the three-phase case. Fix. XXII shows the inter-relation of load resistance and added base resistance, the allowable minimum load resistance to sustain oscillatory operation decreasing as the added base resistance is decreased. This conclusion, predicted by the analysis of this circuit as a relaxation oscillator, is well-substantiated by experimental results.
2. Over the frequency range of application studied in this thesis (7-90 cps), the output frequency of the circuit is directly proportional to the DC input voltage, parasitic time intervals being of no consequence in determining frequency. Furthermore,

the output frequency approaches more nearly the ideal frequency as the total base resistance, reflected into the collector circuit, is increased. The linear relationship between frequency and input voltage, as well as the effect of increasing resistance in the base, is shown in Fig. XVI. Again, this conclusion is predicted by theory and proved experimentally.

3. Because of the importance of minimizing the slope of the negative-resistance portion of the v-i characteristic of the converter as seen from the output terminals, the design of a polyphase switching transistor circuit for maximum power output becomes a delicate balance of compromises, wherein the single most important factor appears to be minimization of component impedances in the circuit. In large measure, this conclusion is based upon the first.
4. The polyphase switching transistor circuit can be used for speed control of induction motors. A synchro with shorted rotor was operated successfully over a range from 950 RPM to 2200 RPM in the experimental work attendant to this thesis. At the present time, the size of motors which can be so controlled, without modifying the circuit arrangement, is limited by the maximum ratings of

power transistors now available. This limitation can be overcome as power transistors of higher rating are developed or by design of an amplifier to amplify the switching-circuit output.

5. The problem of starting an induction motor, made problematical because of the fact that below a certain minimum load impedance relaxation oscillations cannot occur, can be solved by careful design of the circuit, the object of the design being to minimize the negative-resistance slope of the v-i characteristic. In the experimental work attendant to this thesis, a factor of ten reduction in the resistance added to the base for phase-locking resulted in an even greater reduction in the minimum load impedance to sustain oscillatory action.

6. Harmonic content in the applied voltages, while having negligible effect on torque of an induction motor, does produce disproportionate rotor copper losses, thus decreasing motor efficiency and producing undesirable heating. Therefore, the harmonic content should be filtered out of the switching circuit output before applying it to the induction motor. This conclusion is based upon theoretical analysis and was not verified experimentally.

8.2 Recommendations

The following recommendations for further study in the area covered by this thesis are made:

1. Obtain more experimental data concerning circuit operation, particularly as regards speed control of induction motors being supplied by the switching-circuit output.
2. Investigate optimization of switching circuit for maximum power output and maximum power conversion efficiency.
3. Design a filter circuit to remove harmonics from switching-circuit output. Such a circuit must be designed to operate satisfactorily over the frequency range for which speed control is desired.
4. In conjunction with (3), investigate practicability of filtering and amplifying switching-circuit output in order to obtain more power for application to the induction motor.
5. Investigate possibility of designing switching circuit with multiple power transistors to obtain higher power ratings than can be obtained from single transistors [11].

A P P E N D I X

APPENDIX A

PIECEWISE LINEAR ANALYSIS OF THE BASIC CIRCUIT

The purpose of this Appendix is to carry out in detail the analysis of the basic circuit which results in the v-i characteristic of the circuit as shown in Fig. III of Chapter 3 and to show the effect of load on that characteristic. The circuit, as shown in Fig. I, is reproduced in Fig. A-I for convenience.

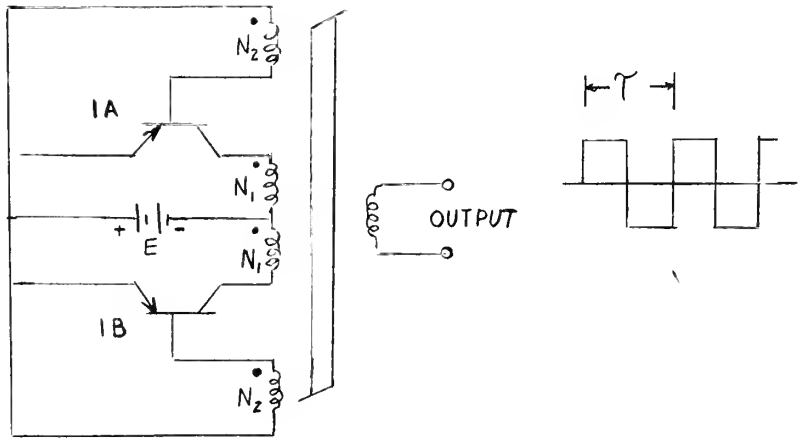

Fig. A-I. Basic switching circuit.

The analysis given in [1] shows that during half of each cycle one transistor is blocking while the other is operating in saturation. Therefore, it is sufficient to examine one-half of the circuit at a time, since the non-conducting side has no effect on the output, provided leakage current is neglected.

To simplify the analysis, leakage inductances of the windings may be neglected and winding resistances included

in the rest of the circuit. Noting then that the conventional piecewise linear model of a transistor is as shown in Fig. A-II, the half of the circuit which is to be analyzed may be represented as shown in Fig. A-III.

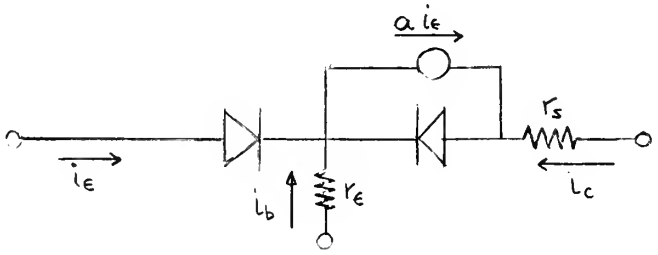

Fig. A-II. Conventional piecewise-linear model of saturated transistor.

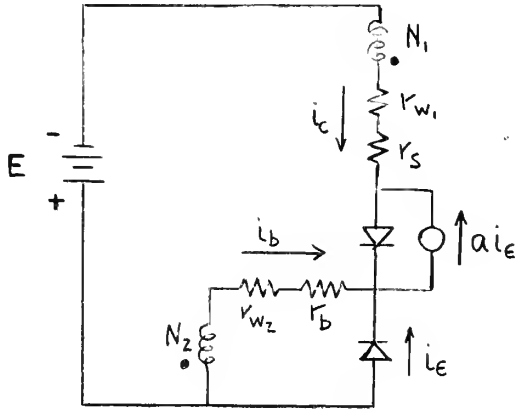

Fig. A-III. Representation of "1A" half of switching circuit with transistor in saturation.

For the moment, regard N_1 and N_2 as ideal transformers and substitute their ideal effects in the circuit as shown in Fig. A-IV.

Then recognize the fact that there is a finite magnetizing inductance and look into the circuit from it; that is, look into the circuit at the N_1 windings from the magnetizing inductance of the N_1 windings. At this point,

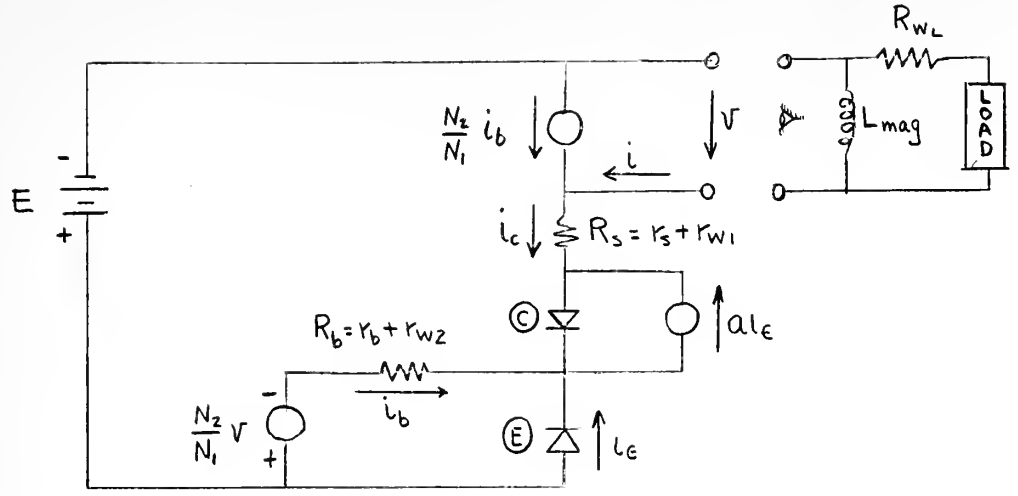

Fig. A-IV. Circuit of Fig. A-III with transformer windings replaced by an ideal voltage source and an ideal current source.

we are ready to proceed with the break-point analysis, the object being to determine the v-i characteristic seen at the terminals indicated in Fig. A-IV. In that figure, (E) designates emitter diode and (C) designates collector diode.

There are three states of interest:

I	(E)	Open	(C)	Open
II	(E)	Closed	(C)	Open
III	(E)	Closed	(C)	Closed

where the diodes are analogous to switches.

In state I, all currents in the circuit are zero, v is negative and of indeterminant magnitude. (This corresponds to the condition wherein the transistor is blocked.)

The next item of interest is the break-point between states II and III. At that point, the collector diode has zero voltage across it and zero current through it. Then, the following equations can be written:

$$i_c = -\alpha i_E \qquad \text{(A-1)}$$

$$i_b = (\alpha - 1) i_E = \left(\frac{1-\alpha}{\alpha}\right) i_c \qquad \text{(A-2)}$$

$$i = i_c - \frac{N_2}{N_1} i_b = i_b \left(\frac{a}{1-a} - \frac{N_2}{N_1} \right) \tag{A-3}$$

$$-v + R_s i_c + E = 0 \tag{A-4}$$

$$i_b = \frac{-N_2 v}{N_1 R_b} \tag{A-5}$$

These equations can be solved for i and v to give the quantities defined as I_o and V_o in Chapter 3:

$$v \triangleq V_o = \frac{E}{1 + \frac{1}{nR_b}\left(\frac{aR_s}{1-a}\right)} \tag{A-6}$$

$$i \triangleq I_o = V_o \left[\frac{1-a(n+1)}{n^2(1-a)R_b} \right] \tag{A-7}$$

from which we obtain:

$$R_o \triangleq \frac{V_o}{I_o} = \frac{n^2(1-a)R_b}{1-a(n+1)} \tag{A-8}$$

This break-point, plus the knowledge that v is zero when i is zero (from State I), defines State II on the v-i characteristic. It is now necessary to determine the v-i characteristic for State III.

In State III, both diodes in the circuit of Fig. A-IV are short circuits. In this case, since we are interested only in the slope of the v-i characteristic, it is most convenient to make an incremental analysis, i.e., E is zero. Then we have:

$$i_b = -\frac{v}{nR_b} \tag{A-9}$$

$$i_c = \frac{v}{R_s} \tag{A-10}$$

$$i + \frac{i_b}{n} - i_c = 0 \qquad \text{(A-11)}$$

from which we can solve for i in terms of v and find:

$$\frac{\Delta v}{\Delta i} = \frac{R_s n^2 R_b}{R_s + n^2 R_b} \qquad \text{(A-12)}$$

With the foregoing information, the v-i characteristic for the upper half of the circuit shown in Fig. A-1 may be constructed as shown in Fig. A-V. Then, if it is recognized that the two halves of the circuit of Fig. A-I are anti-symmetrical, the v-i characteristic for the entire circuit as seen from the magnetizing inductance of the core may be derived by sketching in the other half, as shown in dotted lines in Fig. A-V. The result is the v-i characteristic

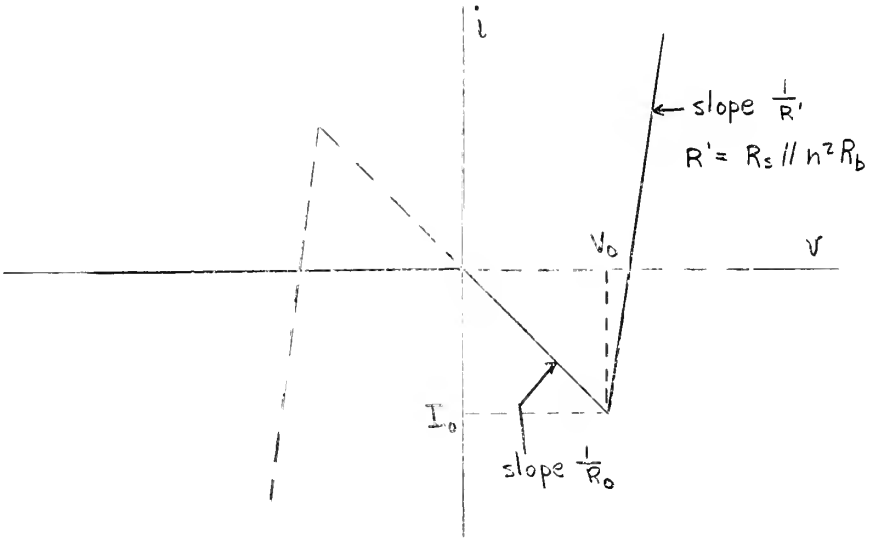

Fig. A-V. v-i characteristic of Basic Switching Circuit.

given in Fig. III of Chapter 3.

With regard to the effect of loads on the operation of the circuit, the most important effect is imposed by a resistance load. The effect is best shown by assuming the magnetizing inductance to be infinite, thus leaving a pure resistive load across the v-i terminals in Fig. A-IV. This may be represented as shown in Fig. A-VI.

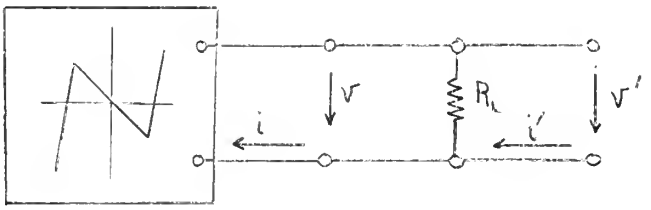

Fig. A-VI. Resistive load placed across terminals of device having known v-i characteristic.

We have:

$$v = v' \tag{A-13}$$

$$i' = i + \frac{v'}{R_L} \tag{A-14}$$

With these relationships, a series of v'-i' characteristics such as are shown in Fig. A-VII can be obtained. It is seen that when $R_L = R_o$ (as R_{L_2} does), the circuit no longer exhibits a negative resistance characteristic, so relaxation oscillations cannot occur.

The effect of inductive loading is, in effect, discussed in Section 3.3 when the core characteristic was regarded as the load on the circuit. It can be seen that the only effect of an additional inductive load would be to change the value

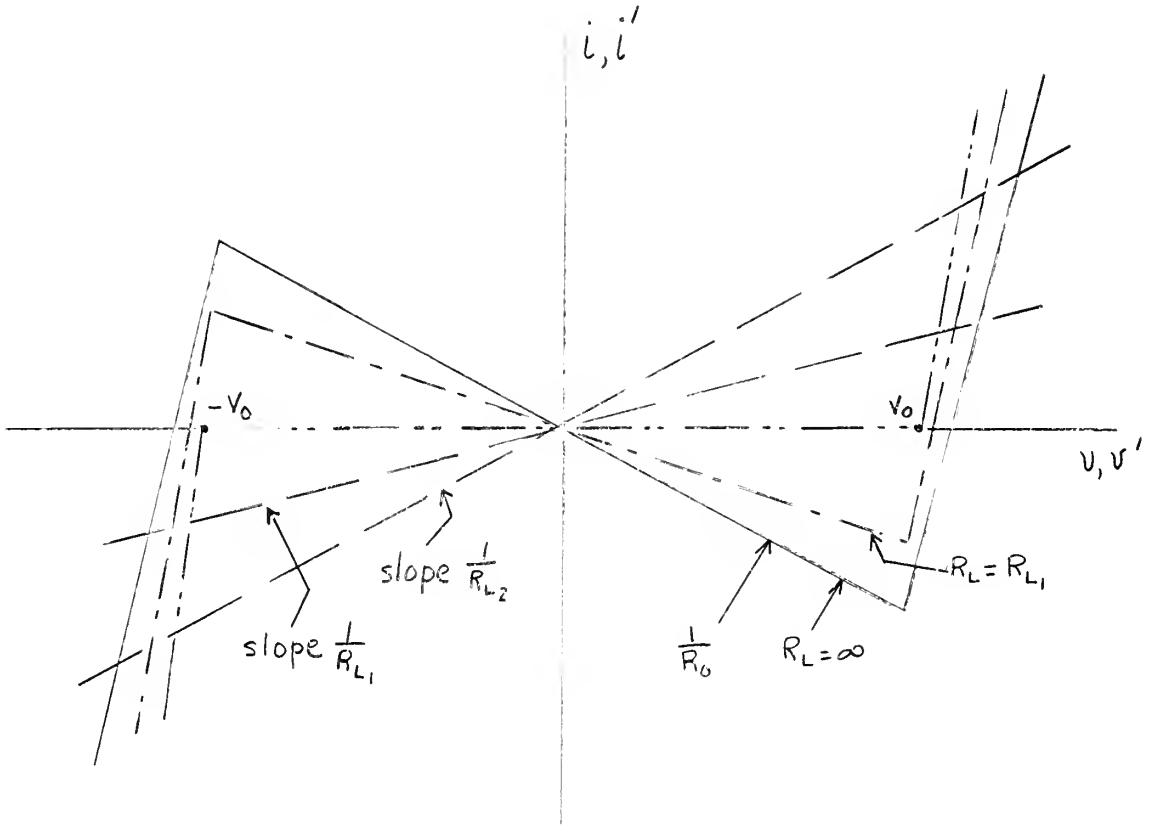

Fig. A-VII. v'-i' characteristic showing effect of resistive load on operation of basic circuit.

of inductance used in Equation (8).

APPENDIX B

CALCULATION OF PARASITIC TIME INTERVALS IN SWITCHING

B.1 Transistor Switching Time

The time intervals of interest in this analysis are the transistor turn-on time, T_o, and the turn-off time. This last is comprised of a storage time, T_1, during which interval the transistor remains saturated, and a decay time, T_2, during which interval the output current decreases to the very small value it has when the transistor is blocking [4]. This current is assumed to be zero.

During the turn-on time, the transistor may be represented by the high-frequency equivalent circuit given by Gray [4] which is shown in Fig. B-I. The frequency-dependent

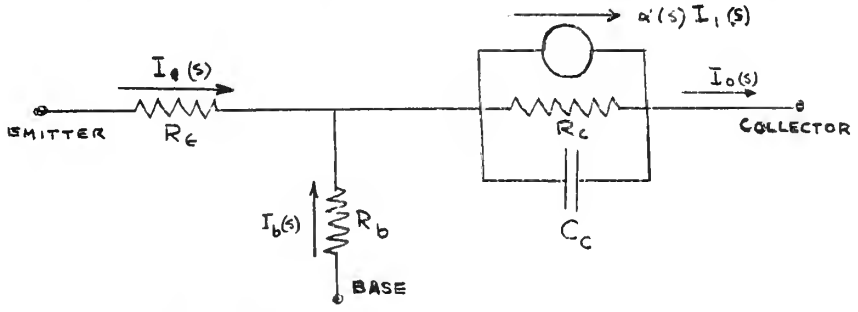

Fig. B-I. High-frequency equivalent circuit of transistor.

current amplification factor shown in this representation is defined as:

$$\alpha(s) = \frac{\alpha_o}{1 + \frac{s}{\omega_o}} \qquad \text{(B-1)}$$

where ω_o is the alpha cut-off frequency. From [4] we have:

$$\frac{I_o(s)}{I_1} = -\frac{\frac{\alpha_o}{1+s/\omega_o} - \frac{R_e}{R_c}\left(1+R_cC_cs\right)}{1-\frac{\alpha_o}{1+s/\omega_o} + \frac{R_e+R_b}{R_c}\left(1+R_cC_cs\right)} \qquad \text{(B-2)}$$

which may be reduced to the following form:

$$\frac{I_o(s)}{I_1} = \left(\frac{\alpha_o - \frac{R_e}{R_c}}{1-\alpha_o+\frac{R_e+R_b}{R_c}}\right)\left[\frac{1-2\xi_1\tau_1 s+\tau_1^2 s^2}{1+2\xi_2\tau_2 s+\tau_2^2 s^2}\right] \qquad \text{(B-3)}$$

where

$$\tau_1 = \sqrt{\frac{R_eC_c}{\omega_o\left(\alpha_o-\frac{R_e}{R_c}\right)}} \qquad \text{(B-4)}$$

and

$$\tau_2 = \sqrt{\frac{(R_e+R_b)C_c}{\omega_o\left(1-\alpha_o+\frac{R_e+R_b}{R_c}\right)}} \qquad \text{(B-5)}$$

Since we are interested only in orders of magnitude of these time constants, we can use values of ω_o and C_c for the H-2 transistor in determining them. Gray gives the following approximate expression for the relation between C_c and V_c [4]:

$$C_c = 1350\, V_e^{-0.8}\ \mu\mu f. \qquad \text{(B-6)}$$

which checks quite well with the collector capacitance information given by the manufacturer for the 2N66 transistor. The minimum capacitance we could expect would then be:

$$C_{c\,min} = 1350(20)^{-0.8} = 1490\ \mu\mu f.$$

A good value for the α cut-off frequency is 200 kilocycles [4]. Based on actual measured parameters for the 2N66 transistors (given in Appendix E), we take the following as average:

$R_e = 1\ \Omega$

$R_b = 50\ \Omega$

$R_c = 12\ K\Omega$

$\alpha_o = .95$

Solving for the time constants of Equations (B-4) and (B-5), we then obtain:

$$\tau_1 = 0.035\ \mu\text{secs.}$$

$$\tau_2 = 1.1\ \mu\ \text{secs.}$$

so we see that the time constants are very small in the turn-on process, from which we can conclude that this time interval is unimportant in the circuit investigated in this thesis.

Now, determination of turn-off time is a more complicated matter. However, it will be of the same order of magnitude as the turn-on time [4]. We therefore state, without proof, that transistor switching time intervals, whether they be turn-on or turn-off intervals, are of negligible importance in the circuit.

B.2 Parasitic Time Interval Due to Non-zero Saturation Inductance of Core

The second, and actually most important parasitic time interval in any cycle is represented by the time required to go from D to G in Fig. B-II (Fig. VI(a) in the Section 3.3, repeated here for convenience). We have the following relations governing the current and voltage along the path of interest:

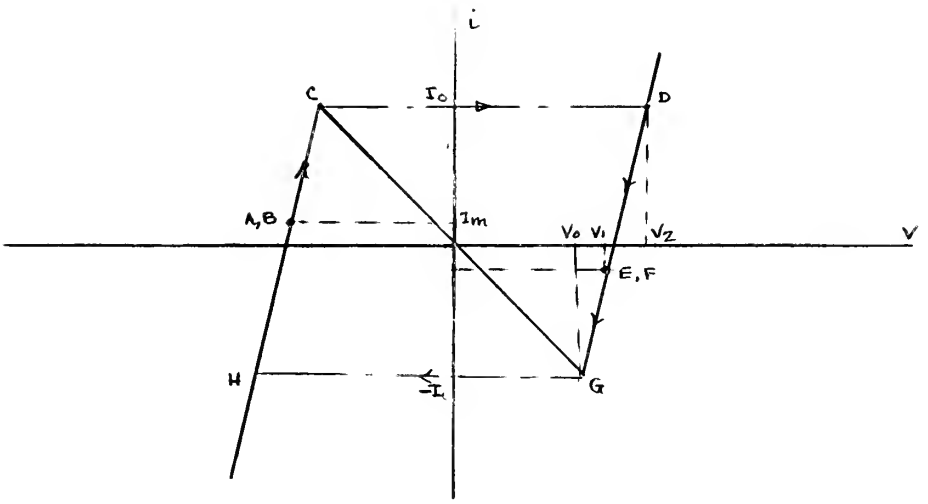

Fig. B-II. v-i characteristic of switching circuit.

$$v = L_s \frac{di}{dt} \tag{B-7}$$

$$v = \left(\frac{R_s n^2 R_b}{R_s + n^2 R_b}\right) i + \frac{E n^2 R_b}{R_s + n^2 R_b} \tag{B-8}$$

Now define:

$$R_p \triangleq \frac{R_s n^2 R_b}{R_s + n^2 R_b} \tag{B-9}$$

Then we have:

$$dt = \left(\frac{L_s}{R_b}\right) \frac{di}{i + \frac{E}{R_s}} \tag{B-10}$$

Integrating between (I_o) and $(-I_o)$, we have

$$\Delta t = \frac{L_s}{R_p} \int_{I_o}^{-I_o} \frac{di}{i + \frac{E}{R_s}} = \frac{L_s}{R_p} \ln\left(i + \frac{E}{R_s}\right)\Bigg|_{I_o}^{-I_o} \tag{B-11}$$

giving:

$$\Delta t = \frac{L_s}{R_p} \ln\left(\frac{\frac{E}{R_s} - I_o}{\frac{E}{R_s} + I_o}\right) \tag{B-12}$$

Now, we can derive an analytical expression for L_s, assuming that at saturation the permeability is that of air:

$$L_s = \frac{N\Phi}{I} = \frac{N^2 BA}{H\ell} = \frac{N^2 \mu_o A}{\ell} \qquad \text{(B-13)}$$

Where A is the effective cross-sectional area and ℓ is the mean length of magnetic path of the core material, both being available from manufacturer's data.

I_o is defined by Equations (1) and (2), repeated here for convenience:

$$I_o = \left[\frac{E}{1 + \frac{a R_s}{n R_b (1-a)}}\right]\left[\frac{1-a(n+1)}{n^2 (1-a) R_b}\right] \qquad \text{(B-14)}$$

Since so many parameters, the precise value of which is not known, are involved in Equation (B-12), any calculation must be, at best, an estimate. However, it should indicate order of magnitude values.

For the circuit used in this thesis, good approximate values of the parameters of interest are:

$a = 0.95$

$R_s = 1$

$n = 320/75 = 4.27$

$R_b = 50$

$A = 2.73$ sq. cm.
$\ell = 23.99$ cm.
} 2.5"x3.5"x1.0" HY MU 80 core

By substituting Equation (B-14) in Equation (B-12) and simplifying, we obtain the following:

$$\Delta t = \frac{L_s}{R_p} \ln \frac{\left\{\frac{1}{R_s} - \frac{1-a(n+1)}{n[nR_b(1-a)+aR_s]}\right\}}{\left\{\frac{1}{R_s} + \frac{1-a(n+1)}{n[nR_b(1-a)+aR_s]}\right\}} \qquad \text{(B-15)}$$

If we substitute the numbers we find:

$$\Delta t = 1.46 \times 10^{-4} \ln \frac{1.0785}{0.9215} = 23\mu \text{ secs.}$$

Again, although of more significant duration than the transistor switching times, the above parasitic time interval is also negligible. Of course, the values of parameters in the above calculation are not precise, but even an order of magnitude error would be insignificant, since, at a maximum frequency of operation of the circuit of 100 cps, the period of one-half cycle is 5000 micro-seconds.

APPENDIX C

PREDICTION OF EFFECT OF PHASE-LOCKING ON OPERATION OF BASIC CIRCUIT

In Section 4.2, it is stated that the addition of the phase-locking circuit increases the slope of the negative-resistance portion of the v-i characteristic of the basic circuit. In this appendix, the equations given there for the two-phase case will be derived.

The circuit under analysis is shown in Fig. C-II. In the analysis, it is assumed that transistors 1A and 2A are conducting, 1B and 2B being blocked. Further, it is assumed that phase relationships are as shown in Fig. C-I.

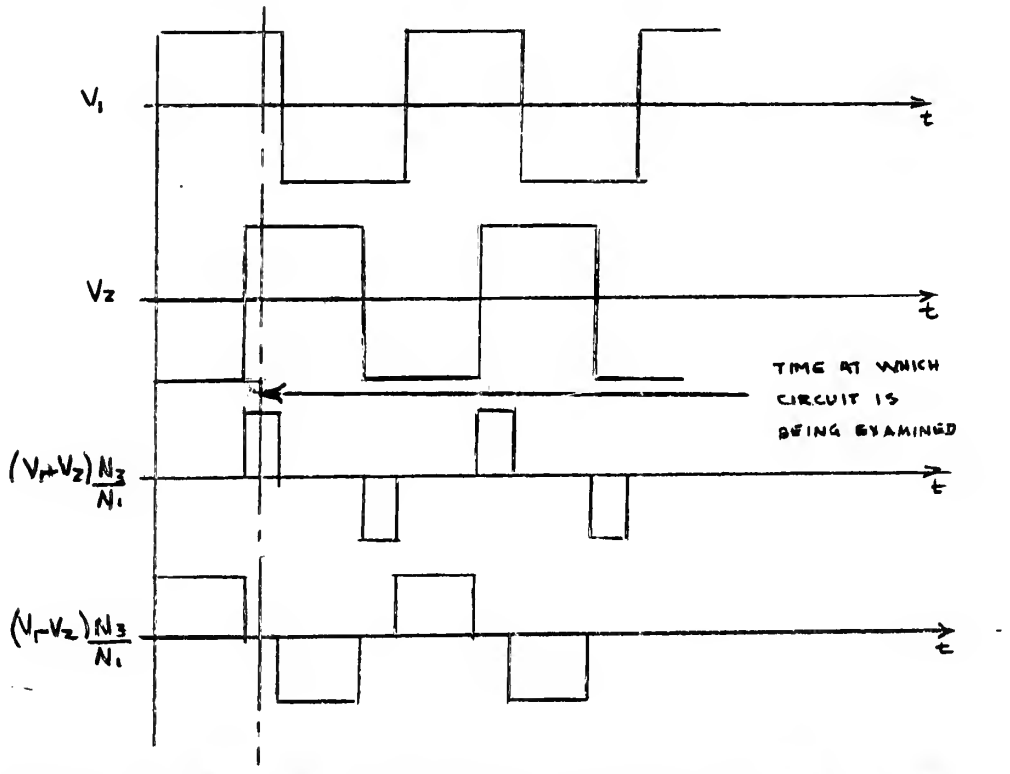

Fig. C-I. Phase relationships in circuit of Fig. C-II.

Fig. C-II

Two-phase circuit for prediction of effect of phase-locking circuit on operation of basic circuit.

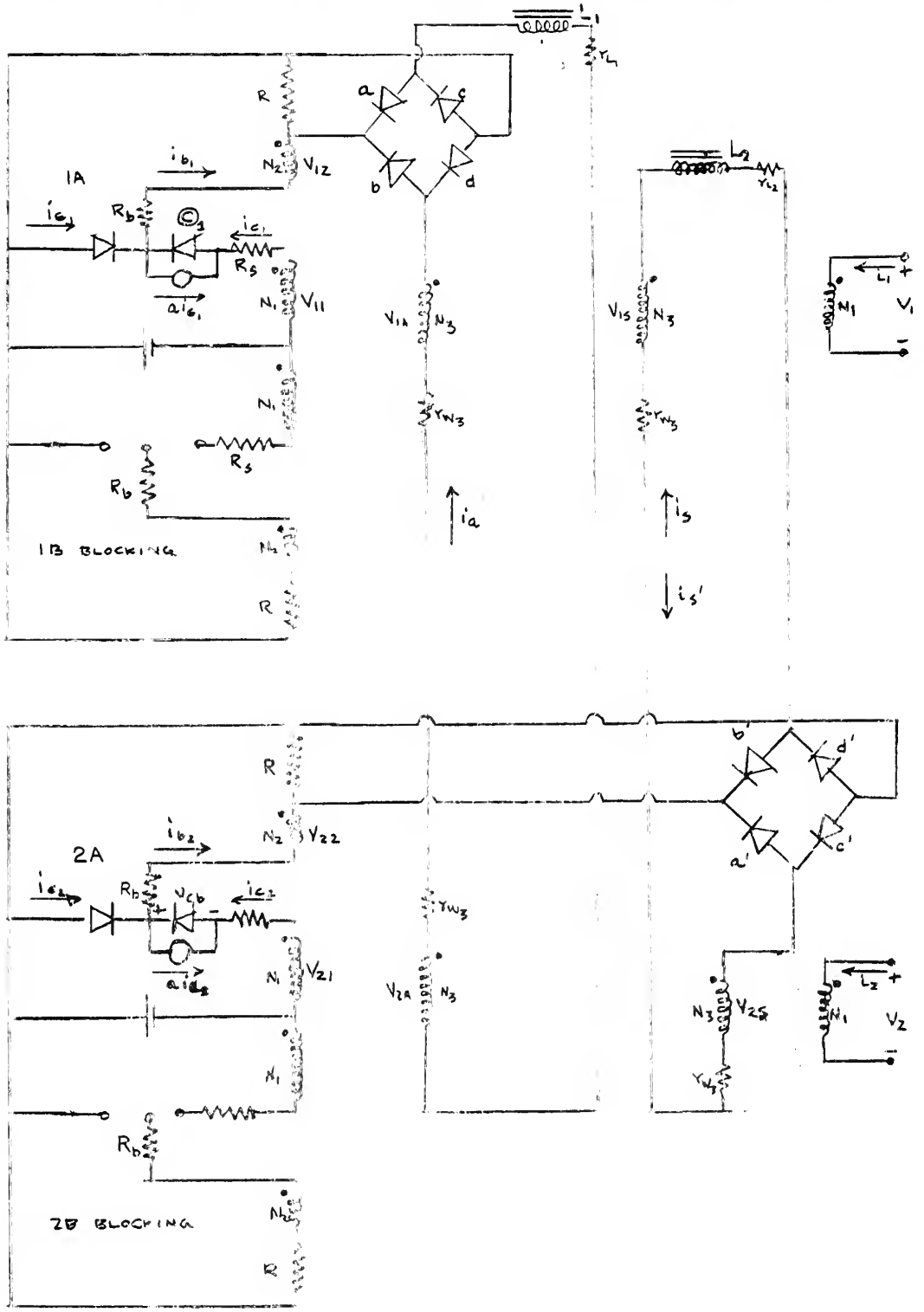

This being the case, we know from the manner of operation of the phase-locking elements that L_1 is unsaturated, whereas L_2 is saturated.

In the circuit of Fig. C-II, there are three indeterminant quantities, viz., i_s, i_a, and V_{cb}. Since, however, L_1 is unsaturated, we can say that:

$$|i_a| = |I_m| \tag{C-1}$$

Furthermore, since:

$$V_{L_1} = L_1 \frac{di_a}{dt} \tag{C-2}$$

we know that the sense of i_a is as shown in Fig. C-II, since the polarity of V_{L_1} must be such that L_1 can absorb most of the voltage induced in the transformer windings of the additive circuit ($V_{L_1} \approx V_{1a} + V_{2a}$).

In order to simplify the analysis, we assume that the reactors, L_1 and L_2, display an ideal square loop characteristic, i.e., there is a finite constant magnetizing current required to saturate them and their saturation inductance is zero. Therefore, at the time in which we are interested, L_2 is a short circuit. Now, the direction of flow of i_s is important. If we assume that it is in the direction shown in Fig. C-II, we have:

$$V_{22} = i_{b_2}(R + R_b) + i_s R \tag{C-3}$$

$$-V_{1S} + V_{2S} + 2(r_{w_3} + r_{L_2}) i_s + (i_{b_2} + i_s) R = 0 \tag{C-4}$$

Note that, in this case, diodes b' and c' are conducting, a' and d' are blocking.

It will be shown that V_{1s} is greater than V_{2s}, but the difference is small. Since the difference involves V_{cb}, an indeterminant quantity, it is not possible to state definitely that Equation (C-4) proves that i_s is in the assumed direction.

If, however, we assume that the current in the subtractive loop is in the opposite direction of i_s, i.e., in the direction of i_s' in Fig. C-II, we have:

$$V_{22} = i_{b_2}(R+R_b) + i_s' R \tag{C-5}$$

$$V_{1S} - V_{2S} + (2r_{w_3} + r_{L_2})\, i_s' + (i_{b_2} + i_s')R = 0 \tag{C-6}$$

In this case diodes a' and d' are conducting, b' and c' are blocking.

Solving Equation (C-6), we obtain:

$$i_s' (2r_{w_3} + r_{L_2} + R) = -(V_{1S} - V_{2S}) - i_{b_2} R \tag{C-7}$$

Again, V_{1s} can be shown to be greater than V_{2s}, so the right hand side of Equation (C-7) is negative. Therefore, the assumed current direction, i_s', is incorrect. From this we can conclude that the actual current is either zero or has some value in the direction of i_s. Essentially what we have is shown in Fig. C-III. In this diagram, the effect of the

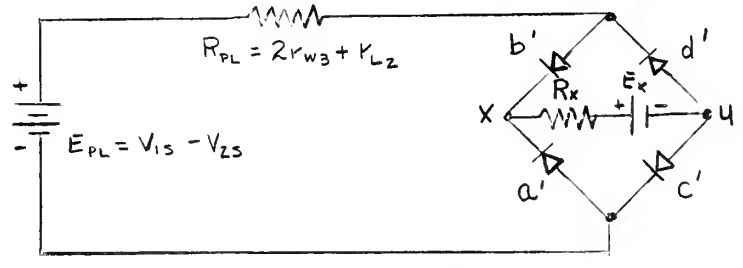

Fig. C-III. Subtractive loop with Thevinin equivalent looking in at R.

converter as seen from the terminals x, y, has been replaced by a Thevinin equivalent voltage source (of the polarity shown) in series with some resistance. The magnitudes of the voltage and resistance need not be determined for an understanding of circuit operation. We see that there is some positive value of E_{P_L} at which the effect of E_x will be overcome and a current, i_s, will flow in the direction shown. If E_{P_L} is less than this amount, all diodes block and no current flows in the circuit. Since E_{P_L} always has the polarity shown (at the time in which we are interested), this confirms the above result which stated that i_s can be zero or have some finite value in the direction shown above.

Therefore, in the analysis which follows, the current in the secondary loop, i_s, will be assumed to have some finite value in the direction shown in Fig. C-II.

We are interested in the break-point at which $\textcircled{C}_1$ in Fig. C-II is on the verge of conducting. Note that the base currents in that diagram are taken in their actual direction of flow, i.e., opposite to the conventional assumed direction. This is because all currents affecting the action of the rectifier bridge must be taken in the direction in which they actually flow. In determining the breakpoint of interest, twenty equations in twenty-three unknowns may be written.

$$\frac{V_1}{N_1} = \frac{V_{1s}}{N_3} = \frac{V_{1a}}{N_3} = \frac{V_{11}}{N_1} = \frac{V_{12}}{N_2} \qquad \text{(C-8)}$$

$$i_1 N_1 - N_3(i_a + i_s) - i_{c_1} N_1 - i_{b_1} N_2 = 0 \qquad \text{(C-9)}$$

$$V_{12} = i_{b_1}(R + R_b) + i_a R \qquad \text{(C-10)}$$

$$-E - i_{c_1} R_s + V_{11} = 0 \qquad \text{(C-11)}$$

$$i_{e_1} - i_{b_1} - a i_{e_1} = 0 \qquad \text{(C-12)}$$

$$a i_{e_1} + i_{c_1} = 0 \qquad \text{(C-13)}$$

$$V_{1a} + V_{2a} - i_a(2r_{w_3} + r_{L_1}) - V_{L_1} - (i_{b_1} + i_a) R = 0 \qquad \text{(C-14)}$$

Note that diodes a and d in the rectifier bridge are blocking, b and c are conducting.

$$V_{1S} - V_{2S} - i_s(2r_{w_3} + r_{L_2}) - (i_{b_2} + i_s) R = 0 \qquad \text{(C-15)}$$

Again, diodes a' and d' are blocking, b' and c' are conducting.

$$V_{22} = i_{b_2}(R + R_b) + i_s R \qquad \text{(C-16)}$$

$$-E - i_{c_2} R_S + V_{21} + V_{cb} = 0 \qquad \text{(C-17)}$$

Note that V_{cb} either has some value in the direction shown in Fig. C-II or is zero. It cannot have a non-zero value in the reverse direction.

$$\frac{V_{22}}{N_2} = \frac{V_{21}}{N_1} = \frac{V_{2a}}{N_3} = \frac{V_{2S}}{N_3} = \frac{V_2}{N_1} \qquad \text{(C-18)}$$

$$i_2 N_1 + i_s N_3 - i_a N_3 - i_{c_2} N_1 - i_{b_2} N_2 = 0 \qquad \text{(C-19)}$$

$$i_{e_2} - i_{b_2} - a i_{e_2} = 0 \qquad \text{(C-20)}$$

$$a i_{e_2} + i_{c_2} = 0 \qquad \text{(C-21)}$$

Equations (C-8) and (C-18) are each actually four equations, so there are, in fact, the twenty equations mentioned earlier. Since there are twenty-three unknowns, explicit solution for any variable is not possible. However, it is possible to solve for v_1 in terms of i_1, so the slope of the negative-resistance portion of the v-i characteristic may be obtained.

In proving the sense of i_s, it was stated that V_{1s} is greater than V_{2s}. By suitable substitutions in the above equations, we find that:

$$V_1 = \frac{E}{1+\frac{a R_s}{n(1-a)(R+R_b)}} + \left(\frac{a}{1-a}\right)\left(\frac{R R_s}{R+R_b}\right)\left[\frac{i_a}{1+\left(\frac{a}{1-a}\right)\frac{1}{n}\left(\frac{R_s}{R+R_b}\right)}\right] \quad (C-22)$$

$$V_2 = \frac{E}{1+\frac{a R_s}{n(1-a)(R+R_b)}} + \left(\frac{a}{1-a}\right)\left(\frac{R R_s}{R+R_b}\right)\left[\frac{i_s}{1+\left(\frac{a}{1-a}\right)\frac{1}{n}\left(\frac{R_s}{R+R_b}\right)}\right] - \frac{V_{cb}}{1+\frac{a R_s}{n(1-a)(R+R_b)}} \quad (C-23)$$

Since i_s is zero in the ideal case and very small in the actual case, certainly being less than i_a, comparison of the above equations shows V_1 to be greater than V_2. Therefore, V_{1s} is greater than V_{2s} as was stated earlier.

We are now interested in solving for i_1 in terms of V_1. From Equations (C-10), (C-12), and (C-13), we have:

$$i_{b_1} = \frac{N_2}{N_1}\left(\frac{V_1}{R+R_b}\right) - i_a\left(\frac{R}{R+R_b}\right) \quad (C-24)$$

$$i_{c_1} = -\frac{a}{1-a}\, i_{b_1} \quad (C-25)$$

Substituting these expressions in Equation (C-9), we obtain:

$$i_1 = \frac{V_1[1-a(n+1)]}{n^2(R+R_b)(1-a)} + i_a\left[\frac{N_3}{N_1} - \frac{[1-a(n+1)]}{n(1-a)}\left(\frac{R}{R+R_b}\right)\right] + i_s\frac{N_3}{N_1} \qquad \text{(C-26)}$$

Taking the ratio of V_1 to i_1 and substituting the expression for V_1 from Equation (C-22) in the resultant equation, the new slope for the negative-resistance portion of the v-i characteristic as seen from the load is found:

$$R_o' = \left(\frac{R+R_b}{R_b}\right)\frac{R_o}{1+K} \qquad \text{(C-27)}$$

$$\text{where } K = \left\{\frac{n\left[n(1-a)(R+R_b)+aR_s\right]}{\left[E+\left(\frac{a}{1-a}\right)\left(\frac{RR_s}{R+R_b}\right)i_a\right]\left[1-a(n+1)\right]}\right\}\left\{i_a\left[\frac{N_3}{N_1} - \frac{[1-a(n+1)]}{n(1-a)}\left(\frac{R}{R+R_b}\right)\right] + i_s\frac{N_3}{N_1}\right\} \qquad \text{(C-28)}$$

Since the quantity $[1-a(n+1)]$ is invariably negative, n being greater than 1, K is normally negative.

Now, from our previous discussion we know that we can substitute I_m for i_a. With regard to i_s, we can argue that physical considerations dictate that it is very small, even less than I_m. Furthermore, the coefficient of i_s in Equation (C-28) is less than the coefficient of i_a. Therefore, we can neglect the term in i_s and write:

$$K \approx \left\{\frac{n\left[n(1-a)(R+R_b)+aR_s\right]}{\left[E+\left(\frac{a}{1-a}\right)\left(\frac{RR_s}{R+R_b}\right)I_m\right]\left[1-a(n+1)\right]}\right\}\left\{I_m\left[\frac{N_3}{N_1} - \frac{[1-a(n+1)]}{n(1-a)}\left(\frac{R}{R+R_b}\right)\right]\right\} \qquad \text{(C-29)}$$

APPENDIX D

DETAILS OF INDUCTION MOTOR ANALYSIS

D.1 Calculation of Currents

In Chapter 6, the effect of harmonic content in applied voltage on torque was determined. However, many steps in the algebra of the solution were omitted. In order that the interested reader may check the accuracy of the final predictions of that chapter, an outline of the solution is given here.

From Section 6.3 (Equations (37), (38), and (39), we have:

$$\begin{bmatrix} \vec{V}_{\alpha_n}^{s} \\ \vec{V}_{\beta_n}^{s} \\ 0 \\ 0 \end{bmatrix} = \begin{bmatrix} Z^{s} & 0 & jn\omega L_{\mu}^{sr} & 0 \\ 0 & Z^{s} & 0 & jn\omega L_{\mu}^{sr} \\ jn\omega L_{\mu}^{sr} & \omega_m L_{\mu}^{sr} & Z^{r} & \omega_m L_{\mu}^{r} \\ -\omega_m L_{\mu}^{sr} & jn\omega L_{\mu}^{sr} & -\omega_m L_{\mu}^{r} & Z^{r} \end{bmatrix} \times \begin{bmatrix} \vec{I}_{\alpha_n}^{s} \\ \vec{I}_{\beta_n}^{s} \\ \vec{I}_{d_n}^{r} \\ \vec{I}_{q_n}^{r} \end{bmatrix} \qquad \text{(D-1)}$$

If we write the system equations from this matrix and then solve by determinants, we obtain equations of the following form:

$$\vec{I}_{\alpha_n}^{s} = \frac{\alpha \vec{V}_{\alpha_n}^{s} - \beta \vec{V}_{\beta_n}^{s}}{\Delta} \qquad \text{(D-2)}$$

$$\vec{I}_{\beta_n}^{s} = \frac{\beta \vec{V}_{\alpha_n}^{s} + \alpha \vec{V}_{\beta_n}^{s}}{\Delta} \qquad \text{(D-3)}$$

$$\vec{I}_{d_n}^{r} = \frac{\gamma \vec{V}_{\alpha_n}^{s} - \delta \vec{V}_{\beta_n}^{s}}{\Delta} \qquad \text{(D-4)}$$

$$\vec{I}_{q_n}^{r} = \frac{\delta \vec{V}_{\alpha_n}^{s} + \gamma \vec{V}_{\beta_n}^{s}}{\Delta} \qquad \text{(D-5)}$$

By Equation (36) of Chapter 6, we have:

$$\vec{V}_{\beta_n}{}^{s} = (-j)^n \vec{V}_{\alpha_n}{}^{s} \tag{D-6}$$

If we substitute this expression in Equations (D-2) through (D-5), we prove the following:

$$\vec{I}_{\beta_n}{}^{s} = (-j)^n \vec{I}_{\alpha_n}{}^{s} \tag{D-7}$$

$$\vec{I}_{q_n}{}^{r} = (-j)^n \vec{I}_{d_n}{}^{r} \tag{D-8}$$

Therefore, we need only solve for $\vec{I}_{\alpha_n}{}^{s}$ and $\vec{I}_{d_n}{}^{r}$ because the other currents may then be obtained from the above equations.

The expressions for $\vec{I}_{\alpha_n}{}^{s}$ and $\vec{I}_{d_n}{}^{r}$ are:

$$\vec{I}_{\alpha_n}{}^{s} = \frac{\vec{V}_{\alpha_n}{}^{s} \begin{vmatrix} Z_n^s & 0 & jn\omega L_\mu{}^{sr} \\ \omega_m L_\mu{}^{sr} & Z^r & \omega_m L_\mu{}^{r} \\ jn\omega L_\mu{}^{sr} & -\omega_m L_\mu{}^{r} & Z_n{}^{r} \end{vmatrix} - \vec{V}_{\beta_n}{}^{s} \begin{vmatrix} 0 & jn\omega L_\mu{}^{sr} & 0 \\ \omega_m L_\mu{}^{sr} & Z_n{}^{r} & \omega_m L_\mu{}^{r} \\ jn\omega L_\mu{}^{sr} & -\omega_m L_\mu{}^{r} & Z_n{}^{r} \end{vmatrix}}{\Delta} \tag{D-9}$$

$$\vec{I}_{d_n}{}^{r} = \frac{\vec{V}_{\alpha_n}{}^{s} \begin{vmatrix} 0 & Z_n^s & jn\omega L_\mu{}^{sr} \\ jn\omega L_\mu{}^{sr} & \omega_m L_\mu{}^{sr} & \omega_m L_\mu{}^{r} \\ -\omega_m L_\mu{}^{sr} & jn\omega L_\mu{}^{sr} & Z_n{}^{r} \end{vmatrix} - \vec{V}_{\beta_n}{}^{s} \begin{vmatrix} Z_n^s & 0 & 0 \\ jn\omega L_\mu{}^{sr} & \omega_m L_\mu{}^{sr} & \omega_m L_\mu{}^{r} \\ -\omega_m L_\mu{}^{sr} & jn\omega L_\mu{}^{sr} & Z_n{}^{r} \end{vmatrix}}{\Delta} \tag{D-10}$$

$$\Delta = Z_n^s \begin{vmatrix} Z_n^s & 0 & jn\omega L_\mu{}^{sr} \\ \omega_m L_\mu{}^{sr} & Z_n^r & \omega_m L_\mu{}^{r} \\ jn\omega L_\mu{}^{sr} & -\omega_m L_\mu{}^{r} & Z_n{}^{r} \end{vmatrix} + jn\omega L_\mu{}^{sr} \begin{vmatrix} 0 & Z_n^s & jn\omega L_\mu{}^{sr} \\ jn\omega L_\mu{}^{sr} & \omega_m L_\mu{}^{sr} & \omega_m L_\mu{}^{r} \\ -\omega_m L_\mu{}^{sr} & jn\omega L_\mu{}^{sr} & Z_n{}^{r} \end{vmatrix} \tag{D-11}$$

In Chapter 6, two quantities were defined as follows:

$$Z_1 \triangleq Z_n{}^{r} Z_n^s - (jn\omega L_\mu{}^{sr})^2 \tag{D-12}$$

$$Z_2 \triangleq \omega_m L_\mu{}^{r} Z_n{}^{s} - jn\omega\omega_m L_\mu{}^{sr\,2} \tag{D-13}$$

Expansion of Equation (D-11) will show that:

$$\Delta = Z_1^2 + Z_2^2 \qquad \text{(D-14)}$$

If then we solve for $\vec{I}_{\alpha_n}^{\,s}$ and $\vec{I}_{d_n}^{\,r}$, the solutions will be of the following form:

$$\vec{I}_{\alpha_n}^{\,s} = \frac{\vec{V}_{\alpha_n}^{\,s}}{Z_n^s}\left[1+\frac{L_\mu^{sr2}}{Z_1^2+Z_2^2}(\zeta - j\eta)\right] \qquad n = 1,5,9\cdots \qquad \text{(D-15)}$$

$$= \frac{\vec{V}_{\alpha_n}^{\,s}}{Z_n^s}\left[1+\frac{L_\mu^{sr2}}{Z_1^2+Z_2^2}(\zeta + j\eta)\right] \qquad n = 3,7,11\cdots \qquad \text{(D-15a)}$$

where $\zeta = n^2\omega^2\omega_m^2 L_\mu^{sr2} - n^4\omega^4 L_\mu^{sr2} + jn\omega\omega_m^2 L_\mu^r Z_n^s - n^2\omega^2 Z_n^r Z_n^s$ (D-16)

and $\eta = jn\omega\omega_m Z_n^r Z_n^s + n^2\omega^2\omega_m L_\mu^r Z_n^s$ (D-17)

$$\vec{I}_{d_n}^{\,r} = \frac{L_\mu^{sr}\vec{V}_{\alpha_n}^{\,s}}{Z_1^2+Z_2^2}\left[\rho + j\sigma\right] \qquad n = 1,5,9\cdots \qquad \text{(D-18)}$$

$$= \frac{L_\mu^{sr}\vec{V}_{\alpha_n}^{\,s}}{Z_1^2+Z_2^2}\left[\rho - j\sigma\right] \qquad n = 3,7,11 \qquad \text{(D-18a)}$$

where $\rho = jn\omega\omega_m^2 L_\mu^{sr2} - jn^3\omega^3 L_\mu^{sr2} - jn\omega Z_n^r Z_n^s - \omega_m^2 L_\mu^r Z_n^s$ (D-19)

and $\sigma = \omega_m Z_n^r Z_n^s - jn\omega\omega_m L_\mu^r Z_n^s$ (D-20)

By simplifying the above expressions for $\vec{I}_{\alpha_n}^{\,s}$ and $\vec{I}_{d_n}^{\,r}$, the following equations can be obtained:

$$\vec{I}_{\alpha_n}^{\,s} = \frac{\vec{V}_{\alpha_n}^{\,s}}{Z_n^s}\left[1-\frac{jn\omega L_\mu^{sr2}(n\omega_m-\omega_m)}{Z_2^2+jZ_1}\right] \qquad n = 1,5,9\cdots \qquad \text{(D-21)}$$

$$\vec{I}^{s}_{\alpha_n} = \frac{\vec{V}^{s}_{\alpha_n}}{Z^{s}_{n}} \left[1 + \frac{jn\omega L_{\mu}^{sr^2}(n\omega+\omega_m)}{-Z_2 - jZ_1} \right] \qquad n = 3,7,11\cdots \qquad \text{(D-21a)}$$

$$\vec{I}^{r}_{d_n} = \frac{L_{\mu}^{sr}\,\vec{V}^{s}_{\alpha_n}(n\omega-\omega_m)}{Z_2 + jZ_1} \qquad n = 1,5,9\cdots \qquad \text{(D-22)}$$

$$= \frac{-L_{\mu}^{sr}\vec{V}^{s}_{\alpha_n}(n\omega+n\omega_m)}{Z_2 - jZ_1} \qquad n = 3,7,11\cdots \qquad \text{(D-22a)}$$

From Equations (D-7) and (D-8) we have that:

$$\vec{I}^{s}_{\beta_n} = -j\vec{I}^{s}_{\alpha_n} \qquad n = 1,5,9\cdots \qquad \text{(D-23)}$$

$$= +j\vec{I}^{s}_{\alpha_n} \qquad n = 3,7,11\cdots \qquad \text{(D-23a)}$$

$$\vec{I}^{r}_{q_n} = -j\vec{I}^{r}_{d_n} \qquad n = 1,5,9\cdots \qquad \text{(D-24)}$$

$$= +j\vec{I}^{r}_{d_n} \qquad n = 3,7,11 \qquad \text{(D-24a)}$$

Equations (D-21) through (D-24a) appear as Equations (42) through (49) in Chapter 6.

D.2 Calculation of Torque

In Chapter 6 the following expression is developed for the electromechanical torque developed in the machine:

$$Te_n = \frac{P}{2} L_{\mu}^{sr}\, \mathcal{R}e\left[-\vec{I}^{s}_{\alpha_n}\vec{I}^{r*}_{q_n} \right] \qquad n = 1,3,5,7\cdots \qquad \text{(D-25)}$$

In order to perform these operations, it is convenient to obtain the following:

$$Z_2 + jZ_1 = -n\omega\left[L_{\mu}^{s}R^{r} + s_n L_{\mu}^{r}R^{s} \right] + jn^2\omega^2\left[\frac{R^{r}R^{s}}{n^2\omega^2} + s_n\left(L_{\mu}^{sr^2} - L_{\mu}^{r}L_{\mu}^{s} \right) \right] \qquad \text{(D-26)}$$

$$Z_2 - jZ_1 = +n\omega\left[L_\mu^{s} R^r + S_n' L_\mu^{r} R^s\right] - jn^2\omega^2\left[\frac{R^r R^s}{n^2\omega^2} + S_n'\left(L_\mu^{sr^2} - L_\mu^{r} L_\mu^{s}\right)\right] \quad \text{(D-27)}$$

where

$$S_n \triangleq \frac{n\omega - \omega_m}{n\omega} \quad \text{(D-28)}$$

$$S_n' \triangleq \frac{n\omega + \omega_m}{n\omega} \quad \text{(D-29)}$$

Then, write the currents as follows:

$$\vec{I}_{\alpha_n}^{s} = \frac{\vec{V}_{\alpha_n}^{s}}{Z_n^{s}}\left[1 + \frac{jn\omega L_\mu^{sr^2}}{A - jB}\right] \qquad n = 1, 5, 9 \cdots \quad \text{(D-30)}$$

$$= \frac{\vec{V}_{\alpha_n}^{s}}{Z_n^{s}}\left[1 + \frac{jn\omega L_\mu^{sr^2}}{A' - jB'}\right] \qquad n = 3, 7, 11 \cdots \quad \text{(D-30a)}$$

$$\vec{I}_{d_n}^{r} = \frac{L_\mu^{sr}\vec{V}_{\alpha_n}^{s}}{-A + jB} \qquad n = 1, 5, 9 \cdots \quad \text{(D-31)}$$

$$= -\frac{L_\mu^{sr}\vec{V}_{\alpha_n}^{s}}{A' - jB'} \qquad n = 3, 7, 11 \quad \text{(D-32)}$$

where

$$A = \frac{L_\mu^{s} R^r}{S_n} + L_\mu^{r} R^s \quad \text{(D-33)}$$

$$B = \frac{R^r R^s}{n\omega S_n} + n\omega\left(L_\mu^{sr^2} - L_\mu^{r} L_\mu^{s}\right) \quad \text{(D-34)}$$

and A' and B' are of the same form except that S_n' replaces S_n.

Now observe that:

$$\vec{I}_{q_n}^{r\,*} = \left(-j\vec{I}_{d_n}^{r}\right)^* = j\vec{I}_{d_n}^{r\,*} \qquad n = 1, 5, 9 \cdots \quad \text{(D-35)}$$

$$= \left(j\vec{I}_{d_n}^{r}\right)^* = -j\vec{I}_{d_n}^{r\,*} \qquad n = 3, 7, 11 \quad \text{(D-35a)}$$

The torques may then be written:

$$T_{e_n} = \frac{P}{2} L_\mu^{sr}\mathcal{R}e\left[-\frac{\vec{V}_{\alpha_n}^{s}}{Z_n^{s}}\left(1 + \frac{jn\omega L_\mu^{sr^2}}{A - jB}\right)\left(\frac{jL_\mu^{sr}\vec{V}_{\alpha_n}^{s}}{-A - jB}\right)\right] \qquad n = 1, 5, 9 \cdots \quad \text{(D-36)}$$

$$= \frac{P}{2} L_\mu^{sr} \mathcal{R}e \left[- \frac{\vec{V}_{an}^{s}}{Z_n^s} \left(1 + \frac{jn\omega L_\mu^{sr^2}}{A' - jB'} \right) \left(\frac{jL_\mu^{sr} \vec{V}_{an}^{s}}{A' + jB'} \right) \right] \qquad n = 3, 7, 11 \cdots \qquad \text{(D-36a)}$$

which may be reduced to:

$$Te_n = \frac{P}{2} \frac{1}{n\omega S_n} \left\{ \frac{\vec{V}_{an}^{s^2} L_\mu^{sr^2} R^r}{\left[\frac{L_\mu^s R^r}{S_n} + L_\mu^r R^s \right]^2 + \left[\frac{R^r R^s}{n\omega S_n} + n\omega \left(L_\mu^{sr^2} - L_\mu^r L_\mu^s \right) \right]^2} \right\} \quad n = 1, 5, 9 \cdots \text{(D-37)}$$

$$- \frac{P}{2} \frac{1}{n\omega S_n} \left\{ \frac{\vec{V}_{an}^{s^2} L_\mu^{sr^2} R^r}{\left[\frac{L_\mu^s R^r}{S_n} + L_\mu^r R^s \right]^2 + \left[\frac{R^r R^s}{n\omega S_n} + n\omega \left(L_\mu^{sr^2} - L_\mu^r L_\mu^s \right) \right]^2} \right\} \quad n = 3, 7, 11 \cdots \text{(D-37a)}$$

D.3 Calculation of Typical Torque-speed Curves

If we arbitrarily assume values of the motor parameters which appear in the torque equations, we can get some idea of the quantitative effect of harmonics on motor action. We assume, then, that:

$$R^r = 0.15\ \Omega$$

$$R^s = 0.30\ \Omega$$

$$L_\mu^{sr} = L_\mu^s = L_\mu^r = 0.04 \text{ henries}$$

$$\omega = 377 \text{ Rad/Sec}$$

$$V = 115 \text{ volts}$$

$$P = 2$$

Substituting these values in Equations (67) and (67a) from Section 6.3, we have:

$$Te_n = \pm \frac{1.37 \times 10^{-2}}{n^3 S_n''} \left\{ \frac{1}{\left[\frac{0.006}{S_n''} + 0.012 \right]^2 + \left[\frac{0.00012}{n S_n''} \right]^2} \right\}$$

where torque is positive for n = 1, 5, 9, etc., and S_n'' is the appropriate slip defined by Equations (64) and (66).

Calculations for various values of motor speed for the fundamental and first two harmonics give the results tabulated in Table D-I.

Table D-I

Numerical Results of Torque-speed Calculations

n	1		3		5	
Motor Speed	S_1	T_1	S_3	T_3	S_5	T_5
1 ω	0	0	1.33	- 1.402	0.80	0.36
0.9 ω	0.1	26.4	1.30	- 1.42	0.82	0.357
0.8 ω	0.2	38.7	1.267	- 1.438	0.84	0.355
0.6 ω	0.4	46.8	1.2	- 1.462	0.88	0.353
0.4 ω	0.6	47.1	1.133	- 1.496	0.92	0.351
0.2 ω	0.8	45.0	1.067	- 1.535	0.96	0.343
0.1 ω	0.9	43.4	1.033	- 1.55	0.98	0.341
0	1.0	42.3	1.000	- 1.565	1.0	0.338

We also desire the maximum torque produced by each of these harmonics. We have:

$$Te_n = \pm \frac{P}{2}\left(\frac{16V^2}{\pi^2}\right)\frac{S_n''}{n^3\omega}\left\{\frac{L_\mu^{sr^2}R^r}{\left[L_\mu^s R^r + S_n'' L_\mu^r R^s\right]^2 + \left[\frac{R^r R^s}{n\omega} + n\omega S_n''\left(L_\mu^{sr^2} - L_\mu^r L_\mu^s\right)\right]^2}\right\} \qquad \text{(D-38)}$$

$$\frac{\partial Te_n}{\partial S_n} = 0 = \left\{\left[L_\mu^s R^r + S_n'' L_\mu^r R^s\right]^2 + \left[\frac{R^r R^s}{n\omega} + n\omega S_n''\left(L_\mu^{sr^2} - L_\mu^r L_\mu^s\right)\right]^2\right\} - S_n''\left\{2L_\mu^r R^s\left[L_\mu^s R^r + S_n'' L_\mu^r R^s\right] + 2\left(L_\mu^{sr^2} - L_\mu^r L_\mu^s\right)\left[R^r R^s + n^2\omega^2 S_n''\left(L_\mu^{sr^2} - L_\mu^r L_\mu^s\right)\right]\right\} \qquad \text{(D-39)}$$

from which the slip for maximum torque may be obtained:

$$S''_{n_{max}} = \pm \sqrt{\frac{n^2\omega^2 R^{r2} L_\mu^{s2} + R^{r2} R^{s2}}{(n\omega L_\mu^r R^s)^2 + \left[n^2\omega^2 L_\mu^r L_\mu^s - (n\omega L_\mu^{sr})^2\right]^2}} \qquad \text{(D-40)}$$

For the parameters assumed above:

$$S''_{n_{max}} = \pm \sqrt{\frac{5.09\,n^2 + 2.02\times10^{-3}}{20.36\,n^2}} \approx 0.5$$

Substituting this value of slip in the torque equation, we have

$$Te_{n_{max}} = \pm \frac{2.74\times10^{-2}}{n^3} \left[\frac{1}{(.024)^2 + \left(\frac{.00024}{n}\right)^2}\right] \approx \pm \frac{47.6}{n^3}$$

for the assumed machine.

So, for the particular machine we have assumed, the harmonic torque maxima are inversely proportional to the cube of the order of the harmonic.

D.4 Calculation of Losses for Slip of 10% Relative to Fundamental

Equation (69) in Chapter 6 gives the expression for rotor power loss due to any harmonic. Substituting the values for the various parameters assumed above, we have:

$$P_{Loss} = \frac{515}{n^2} \left[\frac{1}{\left(\frac{.006}{S_n} + .012\right)^2 + \left(\frac{.00012}{nS_n}\right)^2}\right]$$

When the motor is operating at a slip of 10% relative to the fundamental, this gives the following losses for the fundamental and first two harmonics:

P_{Loss_1} = 1000 watts

P_{Loss_3} = 2080 watts

P_{Loss_5} = 555 watts

The internal mechanical power developed by each harmonic is expressed by the following:

$$P_{int} = (1 - s_n)n\omega T_{en} = \frac{(1 - s_n)}{(s_n)} P_{Loss} \qquad \text{(D-41)}$$

For the fundamental and first two harmonics this gives:

P_{int_1} = 9000 watts

P_{int_3} = 480 watts

P_{int_5} = 122 watts

We see that the efficiency is 90% for the fundamental alone, whereas if we include the first two harmonics, efficiency falls to 72.5%.

APPENDIX E

DESIGN OF POLYPHASE SWITCHING CIRCUIT

The circuit used in the experimental work of this thesis was basically the circuit described by Milnes [2]. In the course of the experimental work, three different sets of cores and two types of transistors were actually used but only one of these circuits is described here.

The first basic limitation on circuit design is that imposed by the transistor characteristics. The transistors used in this circuit were type 2N66 manufactured by Western Electric Co. These are p-n-p alloy type transistors, sealed in a welded can. They were mounted on an unpainted aluminum sheet ($3\frac{1}{2}$"x$3\frac{1}{2}$"x1/16" thick) in order to provide an adequate heat sink. The pertinent characteristics of the 2N66 type are listed below in Table E-I. The parameters of these transistors were measured and are listed in Table E-II.

Table E-I

General Characteristics of 2N66 Transistors

Current, continuous to any electrode	0.8	amps
Maximum collector to emitter voltage	40	volts
Maximum collector to base voltage	60	volts
Reverse current at -4.5 volts, collector to base	75	a
Base voltage for 400 ma collector current	-2.0	volts

Since the limiting collector-to-emitter voltage is -40 volts, the maximum value of control voltage is limited to 20 volts. This is because twice the control voltage appears across the transistor when it is blocking,

The core material used was tape-wound Hy-Mu 80 (tape thickness: 2 mils) manufactured by Magnetics, Inc., and listed as item No. 50042 in their catalogue. These cores have an effective cross section area of 2.73 square centimeters. They are assembled in a protective case with a clear window area of 5.36×10^{6} circular mils. For practical purposes Hy-Mu 80 can be considered to have a maximum flux density of 0.72 webers per square meter. Thus our cores had a maximum flux at saturation of 1.97×10^{-4} webers.

It was decided to design for a frequency of 60 cps of a control voltage of 15 volts. This mean operating point was chosen since the objective of one phase of the experimental work was to apply the output of the switching circuit to a 60 cps induction motor. With these values the number of turns for the collector winding can be obtained from the formula:

$$N_1 = \frac{E}{4 f \Phi_s} = \frac{15}{4 \times 60 \times 1.97 \times 10^{-4}} = 318$$

A value of $N_1 = 320$ turns was selected.

Next it was necessary to determine the load which would be used. Since the power output would be small, it was felt that our induction motor would have to be simulated from available synchro elements. On this basis a resistance of

50 ohms was selected for the load of each phase. This load line is shown plotted on the transistor characteristics in Fig. E-I.

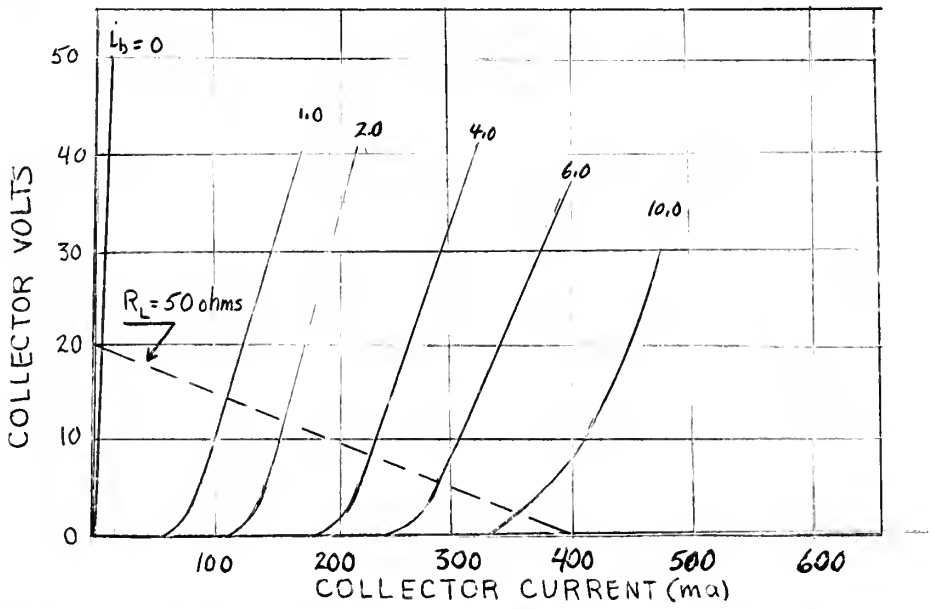

Fig. E-I. Typical output characteristics of a 2N66 transistor in common emitter configuration. (Load line of 50 ohms is shown superimposed.)

From this figure it can be seen that when the converter is operating at 20 volts there will be a collector current of 400 milliamperes. From Table E-I it is seen that for this collector current a base voltage of less than -2.0 volts would be required. Since the base voltage is N_2/N_1 times the collector voltage a turns ratio less than 10 : 1 would be required for the base. However, in order to be assured of cut-off a ratio of about 4 : 1 was chosen. Accordingly 75 turns was used for the value of N_2. This was found to be greatly in excess of the value required, but at the time the circuit was designed the main objective was to

insure operation. If the circuit were to be redesigned in light of present knowledge, a turns ratio of 9 or 9.5 to 1 would be used, the main consideration being to reduce the power dissipation in the base. If the base resistance, R, has to be large for some reason, a smaller value of turns ratio (9 : 1) will reduce the power dissipated and still assure operation.

There is no particular requirement on the turns selected for the coils in the phase locking circuit. Their purpose is to provide voltage for the phase locking circuit. The only consideration should be that they do not provide more volt time area than the saturable reactors can absorb. For the circuit being discussed 150 turns was used for N_3.

The material used for the saturable reactors was Hypernik V, manufactured by Westinghouse. The core used has an effective cross section of 0.69 square centimeters and a maximum flux density of 1.41×10^{-4} webers per square meter.

It has previously been shown in Chapter 4 that the turns for L_1 and L_3, designated N_{L_1} and N_{L_3} are given by Equation (17):

$$N_{L_1} = N_{L_3} = \frac{2N_3}{3} \frac{\emptyset \text{ HYMU 80}}{\emptyset \text{ Hypernik}} = \frac{300}{3} \times \frac{2.73 \times 10^{4} \times .72 \times 10^{-6}}{.69 \times 10^{4} \times 1.41 \times 10^{-6}}$$

$$= 200 \text{ turns}$$

$$N_{L_2} = N_{L_4} = 2N_{L_1} = 400 \text{ turns}$$

Since in reference [3] it was mentioned that the turns for the saturable reactors should be slightly less than the optimum value given above, the windings for the saturable reactors were provided taps to give the following range in turns:

$N_{L_1} = N_{L_3}$ = 130 through 205 in 5 turn steps

$N_{L_2} = N_{L_4}$ = 340 through 410 in 10 turn steps

The rectifier bridges were constructed of the only diodes available in sufficient number, 16 diodes being required for the circuit. The diodes were a silicon type IN336 (0.4 ampere maximum at 120 volts).

Next it was necessary to wind the cores with as large a diameter wire size as possible in order to reduce the winding resistance to a minimum. Since the center core had the greatest number of windings, wire sizes were chosen on this basis. This core required 3 windings of 320 turns, 4 windings of 150 turns, and 2 windings of 75 turns. An upper limit of 400 circular mils per ampere was chosen to limit coil heating. In order to provide for the shuttle used on the winding machine, only one-third of the window area of the cores could be used (1.78×10^6 circular mils). To provide a margin of safety the following allowable currents in the cores were used: N_1 and N_2 - .8 ampere max.

N_3 - 0.5 ampere max.

The winding sizes were then chosen on the basis of making the winding losses equal in all the coils as shown by the calculations below:

Coils	Amp.	Circ.Mils	No. of Coils	Total Turns	Total Circ.Mils
N_1	0.8	x	3	960	960 x
N_2	0.8	x	4	600	600 x
N_3	0.5	5/8 x	2	150	95 x
					1655 x

$$1655\ x = 1.78 \times 10^6 \text{ circular mils (available)}$$

$$x = 1070 \text{ circular mils (use No. 20 awg)}$$

$$5/8\ x = 670 \text{ circular mils (use No. 22 awg)}$$

The saturable reactors had only one winding each and presented no problem. AWG No. 22 was used.

The remaining circuit element, the added base resistance, was originally chosen according to information given in reference [2]. In this it was stated that this resistance should be approximately equal to the inherent base resistance of the transistor. Early in the experimental work, this added resistance was therefore set at 50 ohms, but as further experimental information developed, the base resistance, R, was made a variable.

Table E-II

Measured Parameters 2N66 Power Transistors

Number	α	r_e	r_b	r_c
			Ω	kΩ
D 9437 x	.976	Essentially zero	40.3	144
D 9438 x	.957		50	117.8
D 9439 x	.959		79.5	144
D 40 x	.930		36.7	120.9
D 41 x	.955		39.3	131.1
D 42 x	.923		25.8	127

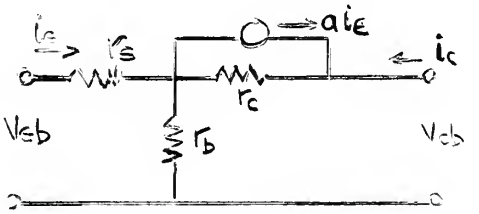

BIBLIOGRAPHY

1. Royer, E. H., A Switching Transistor DC to AC Converter Having an Output Frequency Proportional to the DC Input Voltage, Communication and Electronics, July 1955

2. Milnes, A. G., Phase-Locking of Switching-Transistor Converters for Polyphase Power Supplies, AIEE Advance Paper No. 55-543, presented at AIEE Summer General Meeting, Swampscott, Mass., June 27-July 1, 1955

3. Bright, R. L., Junction Transistors Used as Switches, AIEE Advance Paper No. 55-156, presented at AIEE Winter General Meeting, New York, N. Y., January 31-February 4, 1955.

4. Gray, P. E., Pulse-Circuit Characteristics of Power Transistors, S.M. Thesis, M.I.T., June 1955

5. M.I.T. Course 6.06 Notes, Electric Power Modulators, M.I.T. Electrical Engineering Department Staff, 1955

6. Fitzgerald, A. E., and Kingsley, C., Jr., Electric Machinery, McGraw Hill Book Co., New York, N. Y., 1952

7. Magnetic Circuits and Transformers, M.I.T. Electrical Engineering Department Staff, John Wiley and Sons, Inc., New York, N. Y., 1946

8. Loew, E. A., Direct and Alternating Currents, McGraw Hill Book Co., New York, N. Y., 1946

9. Alger, P. L. The Nature of Polyphase Induction Machines, John Wiley and Sons, Inc., New York, N. Y., 1951

10. M.I.T. Course 6.02 Notes, Electronic Circuits, (Chapter XI, "Relaxation Oscillations"), M.I.T. Electrical Engineering Department Staff, 1954

11. Maisel, L., The Operation of Multiple Power Switching Transistors, S.B. Thesis, M.I.T., January 1956

D662 Dorsey 28795
An analytical and experimental investigation into the application of a polyphase transistor switching circuit for speed contrd of induction motors.